Universidade de Aveiro Departamento de Química
2019

Mónica Isabel Pinto Sousa Ferreira

Oxidação de uma mistura de pequenos compostos aromáticos por UV/H_2O_2 em água da chuva

Oxidation of a mixture of small aromatic compounds by UV/H_2O_2 in rainwater

Universidade de Aveiro Departamento de Química
2019

Mónica Isabel Pinto Sousa Ferreira

Oxidação de uma mistura de pequenos compostos aromáticos por UV/H_2O_2 em água da chuva

Oxidation of a mixture of small aromatic compounds by UV/H_2O_2 in rainwater

Tese apresentada à Universidade de Aveiro para cumprimento dos requisitos necessários à obtenção do grau de Mestre em Biotecnologia, ramo Industrial e Ambiental, realizada sob a orientação científica do Doutor Armando da Costa Duarte, Professor Catedrático do Departamento de Química da Universidade de Aveiro, e da Doutora Patrícia Sofia Matos dos Santos, Investigadora Júnior do Departamento de Química da Universidade de Aveiro.

o júri

presidente

Prof. Doutora Ana Maria Rebelo Barreto Xavier
professora Auxiliar do Departamento de Química da Universidade de Aveiro

Prof. Doutor Mário Miguel Azevedo Cerqueira
professor Auxiliar do Departamento de Ambiente e Ordenamento da Universidade de Aveiro

Doutora Patrícia Sofia Matos dos Santos
investigadora Júnior do Departamento de Química da Universidade de Aveiro

agradecimentos / acknowledgements

Quero agradecer aos meus orientadores, Professor Doutor Armando Duarte e Doutora Patrícia Santos, por todas as orientações, compreensão, amizade e conhecimentos transmitidos ao longo deste trabalho.

Um agradecimento especial aos meus pais, pela oportunidade de ter acesso a uma educação superior e por todos os sacrifícios que fizeram ao longo da vida, e aos meus irmãos, pelo carinho e pelo incentivo. Ao João, pelo apoio incondicional dado durante todo este percurso e por estar sempre presente, tornando esta jornada mais fácil.

Um grande obrigado à Gabriela, pela ajuda e pelo apoio ao longo deste trabalho.

Aos meus amigos, principalmente à Ana Maria, por toda a ajuda, e por terem marcado a minha jornada em Aveiro com momentos memoráveis, e àqueles que, apesar da distância, estiveram sempre presentes.

palavras-chave

Água da chuva, compostos aromáticos, oxidação, processo UV/H_2O_2, otimização, planeamento uniforme, superfície de resposta.

resumo

A água da chuva contém uma enorme variedade de contaminantes, nomeadamente compostos aromáticos, que devem ser removidos se se pretender a respetiva utilização para finalidades domésticas. O presente trabalho avalia a degradação de uma mistura de três pequenos compostos aromáticos (ácidos benzóico, 3,5-dihidroxibenzóico e siríngico), através do processo UV/H_2O_2, em soluções modelo e em água da chuva. A extensão da oxidação foi avaliada por espectroscopias de ultravioleta-visível e fluorescência molecular. Foi verificado que, no decorrer da oxidação da mistura, se formam novos compostos cromofóricos, possivelmente com maior grau de insaturação e hidroxilação, e que posteriormente são degradados. Foi também demonstrado que, o aumento da concentração de H_2O_2, resulta em taxas de oxidação mais elevadas. Por outro lado, foi verificado que o pH não influencia a oxidação da mistura, pelo menos para valores típicos de pH em águas da chuva (entre 4,0 e 7,0). A otimização da oxidação da mistura de contaminantes pelo processo de UV/H_2O_2 foi efetuada através da utilização do "*uniform design"* como planeamento experimental, com os seguintes fatores: concentração de H_2O_2, pH e tempo de reação. O modelo de superfície de resposta corresponde a um polinómio de segunda ordem, onde a extensão de oxidação é função das seguintes variáveis: concentração de H_2O_2, tempo de reação, interação entre estes dois fatores e as respetivas formas quadráticas. A região do ótimo, ou seja, uma extensão de oxidação de aproximadamente 100 %, pode ser observada para uma combinação de valores das variáveis, tendo sido escolhido o ótimo correspondente a uma concentração de H_2O_2 mais baixa (3,1 mM) e ao tempo de reação máximo (4 h). A aplicação das condições ótimas a amostras da água da chuva, às quais foi adicionada a mistura de contaminantes, resultou em extensões de oxidação superiores a 99,5 %, indicando que o modelo é aplicável a amostras reais. Desta forma, os resultados obtidos neste estudo, evidenciam que o processo UV/H_2O_2 pode ser usado como uma alternativa para tratamento de água da chuva, nomeadamente no que diz respeito à remoção de pequenos ácidos aromáticos.

keywords

Rainwater, aromatic compounds, oxidation, UV/H_2O_2 process, optimization, uniform design, response surface model.

abstract

Rainwater contains a large variety of contaminants, namely aromatic compounds, that should be removed if its utilization is intended for domestic purposes. The present work evaluates the degradation of a mixture of three small aromatic compounds (benzoic, 3,5-dihydroxybenzoic and syringic acids), by UV/H_2O_2, in model solutions and in rainwater. The extent of oxidation was assessed by ultraviolet-visible and molecular fluorescence spectroscopies. It was verified that, during the oxidation of the mixture, new chromophoric compounds are formed, possibly with higher degree of unsaturation and hydroxylation, and these compounds are, then, degraded. It was also demonstrated that, the increase of H_2O_2 concentration, results in a higher extent of oxidation. On the other hand, it was verified that the pH does not influence the oxidation of the mixture, at least for pH values in rainwater (between 4.0 and 7.0). The optimization of the oxidation of the mixture of contaminants by the UV/H_2O_2 process was performed through the utilization of the uniform design as experimental design, with the following factors: H_2O_2 concentration, pH, and reaction time. The response surface model corresponds to a second order polynomial, where the extent of oxidation is a function of the following variables: H_2O_2 concentration, reaction time, interaction between these two factors and their respective quadratic forms. The optimum region, which corresponds to an extent of oxidation of approximately 100 %, can be observed for a combination of values for the variables, where the optimum chosen corresponds to a lower H_2O_2 concentration (3.1 mM) and a maximum reaction time (4 h). The application of the optimal conditions to rainwater samples, spiked with a mixture of contaminants, resulted in an extent of oxidation higher than 99.5 %, suggesting that the model is applicable to real samples. The results obtained in this work suggest that the UV/H_2O_2 process can be used as an alternative for the treatment of rainwater, namely in what concerns the degradation of small aromatic acids.

Index

Nomenclature

BA	Benzoic acid
CA	Carbon analyser
CCN	Cloud condensation nuclei
CE-DAD	Capillary Electrophoresis with Diode-Array Detection
DF	Degrees of freedom
DHBA	3,5-dihydroxybenzoic acid
EEM	Excitation-emission matrix
F_{crit}	Critical *F*-value
GC-MS	Gas Chromatography-Mass Spectrometry
HPLC-DAD	High-Performance Liquid Chromatography with Diode-Array Detection
HPLC-MS	High-Performance Liquid Chromatography with Mass Spectrometry
IC-CD	Ion Chromatography with Conductivity Detection
MS	Mean square
PAH	Polycyclic aromatic hydrocarbons
PVC	Polyvinyl chloride
PVDF	Polyvinylidene fluoride
SA	Syringic acid
SL	Sunlight
SS	Sum of squares
t_{crit}	Critical *t*-value
t_{stat}	Calculated *t*-value
UV	Ultraviolet
UV-Vis	Ultraviolet-Visible
VOC	Volatile organic compounds
λ_{exc}	Excitation wavelength
σ	Electrical conduticty

List of figures

List of tables

Chapter 1

Introduction

1.1 Atmospheric waters: general background

Atmospheric water is water that is in the atmosphere under different forms, such as clouds, fogs, rain, dew, and wet aerosol particles. This water comprises about 0.001 % of the natural water resources on the planet, and evaporation from the oceans is the main source of such water (Seinfeld & Pandis, 2006). The transport and phase distribution of atmospheric water is very important for Earth's climate (Seinfeld & Pandis, 2006). In fact, the three states of water (liquid, solid and gaseous or vapor) are present in the atmosphere, which makes the atmosphere the only blanket coating of the planet comprising water in the three aggregate states (Panin, 1990). Furthermore, the interconversion of states of water, such as, evaporation, condensation, sublimation, melting and crystallization, are always occurring in the atmosphere due to the existence of varying pressures and temperatures either in the atmosphere or at the Earth's surface (Seinfeld & Pandis, 2006), which favors the existence of atmospheric water in the different forms.

1.1.1 Importance of atmospheric waters: the role of rainwater

Atmospheric waters have a great importance in atmospheric chemistry, atmospheric radiation, and atmospheric dynamics.

From the different forms of atmospheric water, clouds are dominant in the atmosphere and have a key role in the maintenance of the atmospheric aqueous phase.

Clouds, as well as fogs (which are clouds with a sufficiently extensive ground contact to suppress vertical motions (Pruppacher & Klett, 1978)), are formed due to the presence of particles in the atmosphere (Seinfeld & Pandis, 2006). Such particles, when activated, and in the presence of a supersaturation of water vapor, can grow and form the fog or cloud droplets, and they are named cloud condensation nuclei (CCN; Seinfeld & Pandis, 2006). Therefore, clouds are a major factor in the Earth's radiation budget, as they reflect part of the Sun's radiation back to the space, cover the lower atmosphere and trigger infrared radiation emitted by the Earth's surface (Seinfeld & Pandis, 2006). Clouds also provide a medium for aqueous-phase chemical reactions to occur (producing secondary species) and affect the vertical distribution of species in the atmosphere, which can be scavenged from the atmosphere and arrive to the Earth's surface by wet and dry depositions.

Wet deposition is a natural process by which atmospheric hydrometeors (such as rain and snow) scavenge materials from the atmosphere and carry them to the Earth's surface (Seinfeld & Pandis, 2006). Wet deposition can occur via two mechanisms: rainout and washout (Xing & Chameides, 1990). Rainout refers to the removal of species that are present within the clouds, while washout consists in scavenging species below the clouds by falling hydrometeors (Panin, 2009; Seinfeld & Pandis, 2006; Xing & Chameides, 1990). On the other hand, dry deposition is the process by which materials are transported from the atmosphere into the surface in the absence of precipitation, by wind, direct impaction and gravitational settling (Seinfeld & Pandis, 2006; Tsai et al., 2014). Wet and dry depositions, together, are referred to as bulk deposition (Tsai et al., 2014). From all the precipitation forms, rainwater is the one that occurs more frequently in the Earth, and its content affects the terrestrial and aquatic ecosystems and, consequently, the human life.

1.1.2 Organic compounds in atmospheric waters, namely in rainwater

The composition of atmospheric waters has been the subject of several studies, namely in what regards the organic content. In rainwater, a variety of organic compounds has been found, such as polycyclic aromatic hydrocarbons (PAH) (e.g. Cavalcante et al., 2012; Guo et al., 2014; Thang et al., 2014), volatile organic compounds (VOC) (e.g.

Mullaugh et al., 2015), organic acids (Avery et al., 1991) and carbohydrates (Mullaugh et al., 2014).

Some of the PAHs found in rainwater include fluorene, phenanthrene, anthracene, fluoranthene, pyrene, chrysene, acenaphthene, acenaphthylene, benz[a]anthracene, benzo[a]pyrene, benzo[b]fluoranthene and indeno[1,2,3-cd]pyrene (e.g. Guo et al., 2014). These can derive from anthropogenic and/or biogenic activities, like industrial processes, forest fires, oil refining and burning natural gas, but they are mainly formed by incomplete combustion processes (Liu et al., 2006).

Regarding VOCs, some of the identified in rainwater were: dichloromethane, carbon tetrachloride, 1,2-dichloroethane, 1,1,1-trichloroethane, trichloroethylene, tetrachloroethylene (Okochi et al., 2004), 1,2,4-trimethylbenzene, o-xylene, m,p-xylene (Czuczwa et al., 1988), benzene, ethylbenzene, toluene, methyfuran (Mullaugh et al., 2015). VOCs in rainwater can be originated from anthropogenic activities, such as industrial processes and vehicular emissions, and from biogenic activities, like volcanic emissions (Mullaugh et al., 2015; Salar-García et al., 2016).

Some examples of organic acids present in rainwater include: formic acid, acetic acid (Avery et al., 1991), oxalic acid, lactic acid, succinic acid, malonic acid, pyruvic acid, maleic acid (Avery et al., 2006), benzoic acid (Kawamura & Kaplan, 1986); ethanoic acid and propanoic acid. Organic acids can derive from anthropogenic sources (Arsene et al., 2007) or from the oxidation of organic compounds present in the atmosphere (Santos et al., 2016a).

In what concerns to carbohydrates, sucrose, glucose, levoglucosan, trehalose, fructose, arabinose, galactose, mannitol, arabitol, dulcitol, and levoglucosan (Mullaugh et al., 2014) are some examples of carbohydrates found in rainwater. Their presence in rainwater can derive from anthropogenic sources, like biomass burning (Mullaugh et al., 2014), or biogenic sources, such as microorganisms, animals, plants and fungal spores (Bauer et al., 2008).

As shown above, the organic compounds present in rainwater derive from natural or anthropogenic sources. Fossil fuels, industrial emissions, agriculture and mining are some possible anthropogenic sources, while marine and biogenic aerosols, soil particles and volcanic emissions are some examples of natural sources (Mullaugh et al., 2015; Liu

et al., 2006 . Furthermore, the local of the emissions, the sea level elevation, the pollutant transport processes and the meteorological conditions also affect the composition of rainwater (Arsene et al., 2007; Flues et al., 2002).

1.2 Oxidation processes of organic compounds in atmospheric waters

Oxidation processes are a way of degrading organic contaminants in atmospheric waters. Table 1.1 shows the majority of the studies conducted in this field, organized from the oldest to the newest. Information concerning the organic compounds degraded and the oxidation processes evaluated, as well as the reagents, pH, water type and percentage of oxidation are presented in the Table 1.1.

Table 1.1 evidences that the great majority of the studies were carried out only in model solutions (e.g.: Zuo and Holgné, 1992; Balmer and Sulzberger, 1999; Deng et al., 2006) and only a few were performed in atmospheric waters (Zuo and Holgné, 1994; Zuo et al., 2011; Boris et al., 2015; Santos et al., 2019). The matrix in which the oxidation reaction takes place can influence the degradation of contaminants (due to the presence of other chemical species; (Santos et al., 2019)), and this was not considered in experiments conducted only in model solutions.

The organic compounds whose oxidations were evaluated in the studies present in Table 1.1 were found in atmospheric waters, and they are pointed out as contaminants. Furthermore, the organic compounds and the reagents were used with concentrations similar to the ones found in atmospheric waters. For example, Zuo and Holgné (1992; 1994) used in their works glyoxalic acid, pyruvic acid (which was also studied by Boris et al., (2015)) and oxalic acid (which was also studied by Zuo and Deng (1997)), which are compounds that have been found in rainwater, and are mainly formed by incomplete combustion, ozonolysis, photo-oxidation of hydrocarbons in atmospheric waters or in gas phase (Zuo and Holgné, 1992**;** Zuo and Holgné, 1994). Zuo and Holgné (1992) employed photo-Fenton-like oxidation with UV and sunlight radiations to oxidize oxalic acid, while Zuo and Holgné (1994) used Fe(III) with UV radiation and sunlight radiation to oxidize oxalic acid, glyoxalic acid and pyruvic acid. On the other hand, Boris et al. (2015) used hydrogen peroxide with UV radiation to oxidize pyruvic acid and Zuo and Deng (1997) used Fe(II) and sunlight radiation to oxidize oxalic acid.

Table 1.1: Oxidation processes for the degradation of organic compounds in atmospheric waters found in published work.

Oxidation process	Compound (concentration used; μM)	Reagents (concentration used; μM)	Water type	pH	% oxidation	References
UV/Fe(III)/ H_2O_2	Oxalic acid (1.2×10^2)	$Fe(ClO_4)_3$ (1×10^1)	Model solution	4	N a	Zuo and Holgné, 1992
SL/Fe(III)/ H_2O_2	Oxalic acid (1.2×10^2)	$Fe(ClO_4)_3$ (1×10^1)	Model solution	4	N a	
UV/Fe(III)	Oxalic acid (3×10^1)	$Fe(ClO_4)_3$ (0-1×10^1)	Model solution	4.0	About 80 %[1] (in 9 min; by CA)	Zuo and Holgné, 1994
	Oxalic acid (6×10^1)	$Fe(ClO_4)_3$ (0-1×10^1)	Model solution	4.0	About 80 %[1] (in 9 min; by CA)	
SL/Fe(III)	Oxalic acid (6×10^1)	$Fe(ClO_4)_3$ (1×10^1)	Model solution	4.0	About 42 %[1] (in 7 min; by CA)	
	Oxalic acid (4×10^0)	$Fe(ClO_4)_3$ (0.17×10^1)	Fogwater	3.7	N a	
	Glyoxalic acid (6×10^1)	$Fe(ClO_4)_3$ (1×10^1)	Model solution	4.0	About 97 %[1] (in 7 min; by CA)	
	Pyruvic acid (6×10^1)	$Fe(ClO_4)_3$ (1×10^1)	Model solution	4.0	About 42 %[1] (in 7 min; by CA)	
SL/Fe(II)	Oxalic acid (1.2×10^2)	$Fe(ClO_4)_2.6H_2O$ (1×10^1)	Model solution	3.9	N a	Zuo and Deng, 1997
UV/Fe(II)/ H_2O_2	Atrazine (4.7×10^{-1})	$FeCl_3$ (6×10^0)	Model solution	3.2	About 99.5 %[1] (in 2 h; by HPLC-DAD)	Balmer and Sulzberger, 1999
				4.3	About 99.5 %[1] (in 1 h; by HPLC-DAD)	
				5.6	About 60 %[1] (in 6 h; by HPLC-DAD)	
				7.5	About 0 %[1] (by HPLC-DAD)	
UV/Fe(II)/ H_2O_2	t-butyl methyl ether (5×10^0)	$FeSO_4.7H_2O$ (5×10^0) H_2O_2 (5×10^0)	Model solution	3	About 97 %[1] (in 115 min; by GC-MS)	Guillard et al, 2003
UV	Benzoic acid (1×10^2)		Model solution	3.2	About 100 %[1] (in 150 min; at 254 nm; by CE-DAD)	Deng et al., 2006
					About 60 %[1] (in 210 min; at 300 nm; by CE-DAD)	
UV/Fe(III)	Benzoic acid (1×10^2)	$FeCl_3$ (2×10^1)	Model solution	3.2	About 100 %[1] (in 150 min; at 254 nm; by CE-DAD)	
					About 98 %[1] (in 150 min; at 300 nm; by CE-DAD)	
					About 72 %[1] (in 150 min; at 350 nm; by CE-DAD)	
Vis/Fe(III)	Benzoic acid (1×10^2)	$FeCl_3$ (2×10^1)	Model solution	3.2	About 18 %[1] (in 150 min; at 419 nm; by CE-DAD)	

SL/Fe(III)	Benzoic acid (1×10^2)	$FeCl_3$ (2×10^1)	Model solution	3.2	About 57 %[1] (in 210 min; by CE-DAD)	
UV/Vis	2-nitrophenol (5×10^1–1×10^2)		Model solution	1.7	N a	Vione et al., 2009
				3.7	N a	
				5.9	N a	
				7.8	N a	
				12.6	N a	
	4-nitrophenol (5×10^1–1×10^2)		Model solution	1.7	N a	
				3.7	N a	
				5.9	N a	
				7.8	N a	
				12.6	N a	
UV/Vis/NO_3^-	4-nitrophenol (1×10^2)	$NaNO_3$ (1×10^5)	Model solution	3	N a	
	4-nitrophenol (1×10^2)	$NaNO_3$ (1×10^5)	Model solution	3	N a	
UV	2,4-dinitrophenol (2-1×10^2)		Model solution	2.4	About 75 %[1] (in 165 h; by HPLC-MS)	Albinet et al., 2010
				7.3	About 95 %[1] (in 165 h; by HPLC-MS)	
UV /NO_3^-	2,4-dinitrophenol (2-1×10^2)	$NaNO_3$ (1×10^5)	Model solution	2.5	N a	
				8.7	N a	
UV/Fe(II)/H_2O_2	3-ethoxypropan-1-ol (5×10^1)	H_2O_2 (5×10^1) $FeSO_4.7H_2O$ (5×10^1)	Model solution	3	N a	Carteau and Pichat, 2010
UV/Fe(III)	o-phthalic acid (1×10^1)	$NH_4Fe(SO_4)_2$ (0-2×10^0)	Model solution	2.8	About 100 %[1] (in 60 min; by GC-MS)	Zuo et al. , 2011
				3.7	About 100 %[1] (in 90 min; by GC-MS)	
				4.5	About 100 %[1] (in 120; min by GC-MS)	
			Snow water	4.2	About 35 %[1] (in 120; min by GC-MS)	
UV/H_2O_2	Pyruvic acid (3×10^1-4.6×10^1)	H_2O_2 (1.5×10^2)	Model solution	4.9	About 92 %[1] (in 90 min; by IC-CD)	Boris et al., 2015
			Model solution (with inorganic salts)	N a	About 100 %[1] (in 90 min; by IC-CD)	
			Cloud water (less polluted)	6.2	About 53 %[1] (in 90 min; by IC-CD)	

			Cloud water (more polluted)	6.6	About 100 %[1] (in 90 min; by IC-CD)	
Fe(III)/ H_2O_2	Benzoic acid (2×10^1)	$FeCl_3.6H_2O$ (5×10^0) H_2O_2 (1×10^2)	Model solution	4	About 72 %[1] (in 24 h; by UV-Vis)	Santos and Duarte, 2015
				4.5	About 65 %[1] (in 48 h; by UV-Vis)	
	4-hydroxybenzoic acid (2×10^1)	$FeCl_3.6H_2O$ (5×10^0) H_2O_2 (1×10^2)	Model solution	4	About 90 %[1] (in 24 h; by UV-Vis)	
				4.5	About 88 %[1] (in 24 h; by UV-Vis)	
	3,5-dihydroxybenzoic acid (2×10^1)	$FeCl_3.6H_2O$ (5×10^0) H_2O_2 (1×10^2)	Model solution	4	About 70 %[1] (in 24 h; by UV-Vis)	
				4.5	About 70 %[1] (in 24 h; by UV-Vis)	
				5	About 70 %[1] (in 24 h; by UV-Vis)	
Fe(III)/ H_2O_2	Benzoic acid (2×10^1)	$FeCl_3.6H_2O$ (5×10^0) H_2O_2 (1×10^2)	Model solution	4.5	N a	Santos et al., 2016a
	4-hydroxybenzoic acid (2×10^1)	$FeCl_3.6H_2O$ (5×10^0) H_2O_2 (1×10^2)	Model solution	4.5	N a	
	3,5-dihydroxybenzoic acid (2×10^1)	$FeCl_3.6H_2O$ (5×10^0) H_2O_2 (1×10^2)	Model solution	4.5	N a	
Fe(III)/ H_2O_2	Vanillic acid (2×10^1)	$FeCl_3.6H_2O$ (5×10^0) H_2O_2 (1×10^2)	Model solution	4	80 % (in 24 h; by UV-Vis)	Santos et al., 2016b
				4.5	80 % (in 24 h; by UV-Vis)	
	Syringic acid (2×10^1)	$FeCl_3.6H_2O$ (5×10^0) H_2O_2 (1×10^2)	Model solution	4	80 % (in 24 h; by UV-Vis)	
				4.5	80 % (in 24 h; by UV-Vis)	
				5	N. m.	
SL/Fe(III)	Benzoic acid (2×10^1)	$FeCl_3.6H_2O$ (5×10^0)	Model solution	4.5	About 57 %[1] (in 24 h; by UV-Vis)	Santos et al., 2019
				5	About 19 %[1] (in 24 h; by UV-Vis)	
			Bulk deposition[2] (winter sample)	4.5	About 10 %[1] (in 24 h; by UV-Vis)	
				5	About 18 %[1] (in 24 h; by UV-Vis)	
			Bulk deposition[2] (spring sample)	4.5	About 48 %[1] (in 24 h; by UV-Vis)	
SL/ H_2O_2	Benzoic acid (2×10^1)	H_2O_2 (1×10^2)	Model solution	4.5	About 10 %[1] (in 24 h; by UV-Vis)	
				5	About 15 %[1] (in 24 h; by UV-Vis)	
				4.5	About 15 %[1] (in 24 h; by UV-Vis)	

			Bulk deposition[2] (winter sample)	5	About 8 %[1] (in 24 h; by UV-Vis)
			Bulk deposition[2] (spring sample)	4.5	About 15 %[1] (in 24 h; by UV-Vis)
Fe(III)/ H_2O_2	Benzoic acid (2×10^1)	$FeCl_3.6H_2O$ (5×10^0) H_2O_2 (1×10^2)	Model solution	4.5	About 58 %[1] (in 24 h; by UV-Vis)
			Bulk deposition[2] (winter sample)	4.5	About 25 %[1] (in 24 h; by UV-Vis)
			Bulk deposition[2] (spring sample)	4.5	About 25 %[1] (in 24 h; by UV-Vis)
SL/Fe(III)/ H_2O_2	Benzoic acid (2×10^1)	$FeCl_3.6H_2O$ (5×10^0) H_2O_2 (1×10^2)	Model solution	4.5	95 % (in 24 h; by UV-Vis)
				5	79 % (in 24 h; by UV-Vis)
			Bulk deposition[2] (winter sample)	4.5	66 % (in 24 h; by UV-Vis)
				5	47 % (in 24 h; by UV-Vis)
			Bulk deposition[2] (spring sample)	4.5	84 % (in 24 h; by UV-Vis) 100 % (in 6 h; by molecular fluorescence)

[1]Percentage estimated from a graphic or from a table content.

[2]Bulk deposition = wet and dry depositions

N a = Not available

Guillard et al. (2003) studied the photo-Fenton oxidation of t-butyl methyl ether, which is the most common oxygenated fuel additive used in reformulated gasoline and that can be found in the atmosphere near gasoline stations.

The oxidation of some aromatic acids, such as 4-hydroxybenzoic acid, 3,5-dihydroxybenzoic acid and benzoic acid, which are a tracers from biomass burning (Simoneit, 2002) have also been studied (Deng et al., 2006; Santos and Duarte, 2015; Santos et al., 2016a; Santos et al., 2019). Deng et al. (2006) evaluated the oxidation of benzoic acid by UV photolysis and using Fe(III) with three different types of radiation, namely ultraviolet, sunlight and visible radiation (Deng et al., 2006), while Santos and Duarte (2015; 2016a) used Fenton-like reaction, and Santos et al. (2019) photo-Fenton-like reaction, using sunlight radiation, as well as Fenton-like reaction and Fe(III) with sunlight and hydrogen peroxide with sunlight (Santos et al., 2019). Santos et al. (2016b) evaluated the oxidation of vanillic acid and syringic acid, which are also small aromatic acids, tracers from biomass burning, by Fenton-like reaction, in the absence of light (Santos et al., 2016b).

Vione et al. (2009) studied the oxidation of 2-nitrophenol and of 4-nitrophenol, which are formed as primary pollutants upon emission by combustion processes and as secondary pollutants via phenol nitration, by nitrate photolysis with UV/Vis radiation and by UV/Vis photolysis. On the other hand, Albinet et al. (2010) studied the oxidation of 2,4-dinitrophenol, the most powerful phytotoxic agent in atmospheric hydrometeors that can be derived from mononitrophenols such as the previously mentioned 2-nitrophenol and 4-nitrophenol (Albinet et al., 2010; Vione et al., 2009), by nitrate photolysis with ultraviolet radiation, as well as ultraviolet photolysis.

Carteau and Pichat (2010) evaluated the oxidation of 3-ethoxypropan-1-ol, using photo-Fenton oxidation, with ultraviolet radiation. Zuo et al. (2011) evaluated the oxidation of o-phthalic acid, which is a dicarboxylic acid, the group with the most abundant organic acids in the atmosphere, using Fe (III) and UV radiation (Zuo et al., 2011).

It is important to note that the studies that used Fe(III) or Fe(II) and radiation, i.e. without hydrogen peroxide, assume that hydrogen peroxide is being formed during the reaction, and some studies evaluated its formation, like Zuo & Holgné (1992, 1994) and Zuo & Deng (1997).

The study of Zuo and Holgné (1992) has demonstrated that the sunlight photolysis of Fe(III)-oxalato complexes could be a major source of hydrogen peroxide in the atmospheric liquid phase, and that pH, sunlight intensity and concentrations of oxalate and dissolved iron are related to the formation rate of hydrogen peroxide. It is worth noticing that, under typical conditions for cloudwater, hydrogen peroxide was produced at a significant rate and oxalate was degradaded with a half-life in a few minutes. Hydroxyl radical formation in cloudwater was influenced by the photolysis of Fe(III)-oxalato complexes.

Zuo and Holgné (1994) suggested that the degradation rate of oxalic acid and α-keto acids by Fe(III)-catalyzed photochemical increased with sunlight intensity, with the concentration of Fe(III) and with the concentration of substrate.

Zuo and Deng (1997) indicated that the Fe(II)/Fe(III) couple is involved in the decomposition of oxalic acid and formation of hydrogen peroxide, and that Fe(III) is the most active catalyst species. Their work suggests that, since the photochemical cycling between Fe(II) and Fe(III) occurs rapidly in the atmospheric droplets, the initial oxidation state of iron is not critical for the catalytical processes.

According to the work of Balmer and Sulzberger (1999), Fe(III) and pH affect the rate of hydroxyl radicals formation and the kinetics of atrazine degradation by hydroxyl radicals produced in photo-Fenton systems. The results regarding the effects of pH show that photo-Fenton systems are inefficient at neutral and basic pH's, even when organic complexing compounds are present, mostly due to the effect of pH on Fe(III) speciation. In atmospheric waters, with low pH, the efficiency of contaminants degradation by these processes depends on the presence of organic complexing agents and on their concentration. For example, organically complexed Fe(III) is more efficiently photolyzed than inorganic Fe(III) and organically complexed Fe(II) is faster oxidized. Moreover, organic complexing agents can also act as hydroxyl radical scavengers.

Deng et al. (2006) claims that benzoic acid can undergo a rapid photodegradation under solar irradiation in the presence of Fe(III) and that its degradation rate increased with increasing the concentration of Fe(III). Furthermore, the degradation of benzoic acid was shown to be more efficient when the pH of the system was lower than 4.

Vione et al. (2009) studied several processes for the oxidation of nitrophenols and concluded that reaction with hydroxyl radicals would be the fastest removal process for these compounds. Reaction with $^{\cdot}NO_3$ and direct photolysis were other studied processes, which showed to be slower than the reaction with hydroxyl radicals. Another author who has published work in the phototransformation of nitrophenols was Albinet et al. (2010), whose work shows that the direct photolysis and the reaction with hydroxyl radical play a comparable role in the degradation of 2,4-dinitrophenol at pH's higher than 4. However, the hydroxyl reaction would prevail for pH's lower than 4. Both processes are reported to be more important than the reaction with $^{\cdot}NO_3$ in the absence of light for the degradation of 2,4-dinitrophenol in atmospheric waters.

According to Zuo et al. (2011), who have studied the photochemical degradation of phtalic acid, the direct photodecomposition of this acid is slow, nonetheless, the addition of Fe(III) causes the acceleration of the light-induced degradation of phtalic acid, which increases by decreasing the pH value to values between 2.8 and 4.5.

The Fenton-like oxidation of vanillic and syringic acids has been studied by Santos et al. (2016b), which suggests that the oxidation of these acids is affected by the pH of the solutions, wherein the oxidation rate increased with the decrease of the pH. This implies that more acidic pH's accelerate the Fenton-like oxidation of these acids. UV-Vis and fluorescence data demonstrated that the vanillic and syringic acids were degraded by Fenton-like oxidation, but not totally degraded within 24 h in the absence of light. Other studies of Santos et al. (2015; 2016a), where the oxidation of benzoic, 4-hydroxybenzoic and 3,5-dihydroxybenzoic acids was studied, also revealed that the night period may not be sufficient for the complete degradation of these compounds in the atmospheric waters, and that pH affects the extent of the oxidation of these compounds.

The oxidation of benzoic acid was also studied by different oxidation agents, namely Fe(III), hydrogen peroxide, sunlight, and combinations of these agents, by Santos et al. (2019). The results showed that the extent of oxidation increased with the decrease of the pH value, which is in accordance with other studies (e.g. Santos & Duarte, 2015), and that the utilization of sunlight simultaneously with other oxidation agents increased the oxidation of benzoic acid, which reveals the importance of the hydroxyl radicals for these reactions.

This study resulted in the total oxidation of benzoic acid after 6 h in a spring rainwater sample, and in the almost total oxidation after 24 h in a winter rainwater sample.

Most of the oxidation reactions presented in Table 1.1 have the hydroxyl radical ($OH^{\cdot}$) as the active oxidizing agent. Moreover, among the most studied oxidation reactions in atmospheric waters were found the Fenton and photo-Fenton reactions (e.g. Guillard et al., 2003), the Fenton-like (e.g. Santos & Duarte, 2015) and photo-Fenton-like reactions (e.g. Zuo & Holgné, 1992), the nitrate photolysis (e.g. Albinet et al., 2010) and the UV photolysis (e.g. Deng et al., 2006), which are following presented in Table 1.2.

The name of Fenton reaction came from Henry J. H. Fenton, who developed in the 1890s the Fenton reagent, comprising iron (III) ions in the presence of certain oxidizing agents (Fenton, 1894). Nowadays, the Fenton reagent is defined as a solution of hydrogen peroxide (H_2O_2) with ferrous iron (Fe^{2+}) as catalyst, and it is used for the oxidation of organic pollutants (Bokare & Choi, 2014). In the Fenton oxidation process, iron (II) (Fe^{2+}) is oxidized by H_2O_2 to iron (III) (Fe^{3+}), forming a hydroxyl radical ($OH^{\cdot}$) and a hydroxide ion (OH^{-}). Fe^{3+} is then reduced back to Fe^{2+} by another molecule of H_2O_2, originating a hydroperoxyl radical ($HOO^{\cdot}$) and a proton (H^{+}). In the presence of an organic compound (R-H), $OH^{\cdot}$ abstracts a hydrogen atom from such compound, leading to the formation of an organic radical ($R^{\cdot}$), which undergoes a series of chemical reactions, forming several reaction products (Bokare & Choi, 2014). The utilization of an excess of H_2O_2 and Fe^{2+}, in the absence of any competitive scavenging of $OH^{\cdot}$ and $R^{\cdot}$, should culminate in the oxidation of the organic compounds to primarily carbon dioxide (CO_2) and water (H_2O) (Bokare & Choi, 2014). The kinetics of the Fenton reaction is influenced by the pH of the solution, as it depends on the simultaneous presence in solution of dissolved Fe^{2+} and Fe^{3+}, and the solubilities of both ions have an impact on the kinetics of the reaction. In natural water, at near neutral pH's, Fe^{2+} is more soluble than Fe^{3+}, which means that Fe^{3+} is the limiting factor for the reaction rate. At acidic pH's, the reaction proceeds rapidly, and, at basic pH's, the reaction is slower due to the precipitation of $Fe(OH)_3$, which lowers the concentration of Fe^{3+} in solution (Pignatello et al., 2006).

Table 1.2: Oxidation processes that can occur in atmospheric waters and respective main reactions.

Oxidation process	Reactions	Reference
Fenton reaction	$Fe^{2+} + H_2O_2 \rightarrow Fe^{3+} + OH^{\bullet} + OH^-$	(Hardwick, 1957)
	$Fe^{3+} + H_2O_2 \leftrightarrow Fe(O_2H)^{2+} + H^+$	(Walling & Weil, 1974)
	$Fe(O_2H)^{2+} \rightarrow Fe^{2+} + OOH^{\bullet}$	(Walling & Weil, 1974)
	$OH^{\bullet}$ + organic compound → oxidation products	
Photo-Fenton reaction	$Fe^{2+} + H_2O_2 + h\nu \rightarrow Fe^{3+} + OH^{\bullet} + OH^-$	(Hardwick, 1957)
	$Fe^{3+} + H_2O + h\nu \rightarrow Fe^{2+} + OH^{\bullet} + H^+$	(Ruppert et al., 1993)
	$Fe^{2+} + OH^{\bullet} \rightarrow Fe(OH)^{2+}$	(Safarzadeh-Amiri et al., 1996)
	$Fe(OH)^{2+} + h\nu \rightarrow Fe^{2+} + OH^{\bullet}$	(Baxendale & Magee, 1954)
	$H_2O_2 + h\nu \rightarrow 2OH^{\bullet}$	(Downes & Blunt, 1879)
	$OH^{\bullet}$ + organic compound → oxidation products	
Fenton-like reaction	$Fe^{3+} + H_2O_2 \rightarrow Fe(O_2H)^{2+} + H^+$	(Walling & Weil, 1974)
	$Fe(O_2H)^{2+} \rightarrow Fe^{2+} + OOH^{\bullet}$	(Walling & Weil, 1974)
	$Fe^{2+} + H_2O_2 \rightarrow Fe^{3+} + OH^{\bullet} + OH^-$	(Hardwick, 1957)
	$OH^{\bullet}$ + organic compound → oxidation products	
Photo-Fenton-like reaction	$Fe^{3+} + H_2O_2 + h\nu \rightarrow Fe(O_2H)^{2+} + H^+$	(Lee & Yoon, 2004)
	$Fe(O_2H)^{2+} \rightarrow Fe^{2+} + OOH^{\bullet}$	(Walling & Weil, 1974)
	$Fe^{2+} + H_2O_2 \rightarrow Fe^{3+} + OH^{\bullet} + OH^-$	(Hardwick, 1957)
	$Fe^{3+} + H_2O \rightarrow FeOH^{2+} + H^+$	(Milburn & Vosburgh, 1955)
	$FeOH^{2+} + h\nu \rightarrow Fe^{2+} + OH^{\bullet}$	(Lee & Yoon, 2004)
	$H_2O_2 + h\nu \rightarrow 2OH^{\bullet}$	(Downes & Blunt, 1879)
	$OH^{\bullet}$ + organic compound → oxidation products	
Nitrate photolysis	$NO_3^- + h\nu \rightarrow NO_3^{-*}$	(Mack & Bolton, 1999)
	$NO_3^{-*} \rightarrow NO_2^{\bullet} + O^{-\bullet}$	(Mack & Bolton, 1999)
	$NO_2^{\bullet} + O^{-\bullet} + H^+ \rightarrow NO_2^{\bullet} + OH^{\bullet}$	(Mack & Bolton, 1999)
	$OH^{\bullet}$ + organic compound → oxidation products	
UV photolysis	$H_2O_2 + h\nu \rightarrow 2OH^{\bullet}$	(Downes & Blunt, 1879)
	$OH^{\bullet}$ + organic compound → oxidation products	

The photo-Fenton reaction differs from Fenton reaction by the irradiation of the solution by UV or solar light, which enhances the production of $OH^{\cdot}$ (Bokare and Choi, 2014). This is achieved through the photoreduction of Fe^{3+} to Fe^{2+}, combined with the photolysis of H_2O_2 (Bokare and Choi, 2014). Fe^{2+} ions are recycled continuously by irradiation, and, thus, are not depleted during the oxidation reaction and the photo-reduction of Fe^{3+} to Fe^{2+} ions is promoted along with the generation of additional $OH^{\cdot}$ (Sarrai et al., 2016).

Similar to Fenton reaction, Fenton-like reaction is a reaction between H_2O_2 and Fe, but instead of Fe^{2+}, it uses Fe^{3+}. The photo-Fenton-like reaction, like in the case of photo-Fenton, makes use of UV or solar light and, thus, has a higher degree of oxidation than the reaction in the absence of light (Pignatello et al., 2006). This process also employs Fe^{3+} and H_2O_2 in acid conditions (Lumbaque et al., 2019).

The Fenton and related reactions are viewed as potentially convenient and economical ways to generate oxidizing species for the degradation of contaminants (Pignatello et al., 2006). Hydrogen peroxide (H_2O_2), one of the reagents used in Fenton and related reactions, when compared to other bulk oxidants, is safe, inexpensive, easy to handle, and does not pose a lasting environmental threat as it readily decomposes into water and oxygen (Pignatello et al., 2006). Iron, the other reagent used in Fenton and related reactions, is inexpensive, safe and environmentally friendly (Pignatello et al., 2006). Moreover, iron is the fourth most abundant metal that can be found in the Earth's crust, and can be found in the forms of Fe^{2+} or Fe^{3+} ions (Safarzadeh-amiri et al., 1996). This metal can also be found in aerosols, fogs and rain drops due to the wind, which is able to transport iron to the atmosphere (Safarzadeh-amiri et al., 1996).

In the case of the nitrate photolysis, generally nitrate is used as a source of $OH^{\cdot}$ in the presence of UV light (Mack & Bolton, 1999).

The UV photolysis, in the presence of H_2O_2 (UV/H_2O_2), generates $OH^{\cdot}$, which oxidize certain organic compounds as well (Mack & Bolton, 1999). One advantage of using the UV/H_2O_2 process for water treatment is the fact that UV light can work simultaneously as a disinfectant (Vione et al., 2006).

1.3 Purpose of the work: oxidation of organics in rainwater

Rainwater is a relatively clean water source, and, with necessary caution, it can be used for various purposes, like garden watering, laundry and cooling and heating (Rahman et al., 2019). It can be harvested in a substantial quantity from roof catchments and other pavement areas, which plays an important role in water sustainability by reducing the pressure on main water supplies (Rahman et al., 2019). Before its use, however, some contaminants should be removed from the water, as they could cause harm to human health.

The oxidation of organic contaminants is one way of removing them from the rainwater. To the best of my knowledge, only Santos et al. (2019) studied the oxidation of organic contaminants in rainwater, and only for a single organic compound (benzoic acid). Therefore, the aim of this work was to evaluate the degradation of a mixture of organic contaminants in rainwater, namely the benzoic acid, the 3,5-dihydroxybenzoic acid and the syringic acid (Figure 1.1) at environmentally relevant concentrations, by an oxidation process which combines hydrogen peroxide with UV light (UV/H_2O_2). These contaminants were chosen since they are aromatic compounds, are tracers of biomass burning (Simoneit, 2002), and they were found in aqueous extract of biomass burning aerosol (Graham et al., 2002). In addition, the effects of H_2O_2 concentration, of pH, and time of reaction on the oxidation were assessed. The optimum conditions for the oxidation of the mixture of contaminants were found using uniform design and response surface model. The experiments were performed in model water solutions and in rainwater samples. The degradation of contaminants was evaluated by Ultraviolet-Visible (UV-Vis) and molecular fluorescence spectroscopies.

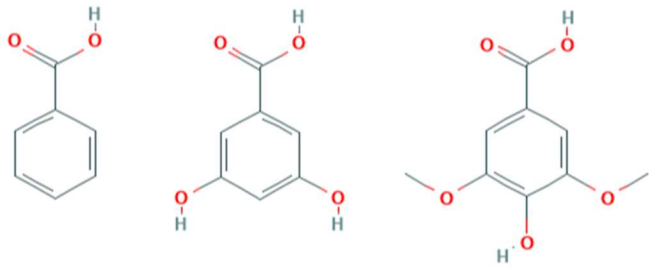

Figure 1.1: Chemical structure of benzoic acid (left), of 3,5-dihydroxybenzoic acid (middle) and of syringic acid (right).

Chapter 2

Material and methods

2.1 Experimental procedure

The oxidation of a mixture of compounds containing benzoic acid, 3,5-dihydrozybenzoic acid, and syringic acid, each one with a concentration of 0.02 mM, was performed in water model solutions, under UV radiation (254 nm) and in the presence of H_2O_2 (UV/H_2O_2 process). Solutions were freshly prepared from stock solutions of benzoic acid (10 mM), of 3,5-dihydrozybenzoic acid (10 mM), of syringic acid (2 mM), and of H_2O_2 30 % (w/w). The oxidation, in a similar way, was also performed for the individual compounds as a control. The effects of the H_2O_2 concentration and of the pH, as well as of the time of reaction, on the oxidation of the mixture of the compounds were assessed by UV-Vis and molecular fluorescence spectroscopies. After the preparation of the solutions containing the organic compounds, the pH of the solutions was always measured, and adjusted with H_2SO_4 (0.1 M) and $NaHCO_3$ (0.1 M) solutions. A pH meter with a glass Jenway pH electrode (model 924 005) was used and calibrated each day of experimental work with pH 4 and pH 7 buffers. After adjustment of pH, 20 mL of the solutions were transferred to quartz test tubes, H_2O_2 was added, and, immediately after, the tubes were put under a 6 W UV lamp emitting at 254 nm, in an incubator at (20 ± 2) ºC, to initiate the oxidation reactions.

To assess the effect of the time of reaction, after adjustment of pH to 5.6 (neutral pH for rainwater), H_2O_2 was added to obtain an initial concentration of 0.5 mM, and the oxidation was evaluated for the following reaction times: 0 h, 0.5 h, 1 h, 1.5 h, 2 h, 3 h, 4 h, 5 h, 6 h and 7 h. At least three replicates of the above procedure, for the mixture of compounds and for each compound individually, were made in different days.

In order to evaluate the influence of the concentration of H_2O_2 in the oxidation of the mixture of compounds, three different concentrations of H_2O_2 were tested, namely: 0.5 mM, 2.5 mM and 5.0 mM. The steps were the same as referred above, and the oxidation was evaluated for 0 h, 1 h, 2 h and 4 h.

To test the influence of pH on the oxidation of the mixture of compounds, three different initial pH's were used, namely, 4.0, 5.6 and 7.0, which are acid, neutral, and basic pH values for atmospheric waters, respectively (Seinfeld and Pandis, 2006). The concentration of H_2O_2 was fixed at 5.0 mM, and the oxidation was evaluated for 0 h, 1 h, 2 h, 3 h and 4 h. At least three replicates were made for each pH.

Prior to use, all glass material was immersed in a solution of NaOH (0.1 M) for 30 min, and, then, rinsed with distilled water, followed by another immersion in a solution of HNO_3 (4 M) for 24 h, after which the materials were rinsed with distilled water and with ultrapure water.

2.2 Optimization process of the oxidation of contaminants by UV/H_2O_2

For the optimization of the removal of contaminants by UV/H_2O_2, the uniform design was used as experimental design, and three levels for three factors were defined. The factors were the reaction time, the H_2O_2 concentration and the pH of solution, and the levels used were the following: 2 h, 4 h and 7 h, for the time of reaction; 0.5 mM, 2.5 mM and 5.0 mM, for the H_2O_2 concentration; and 4.0, 5.6 and 7.0, for the pH of solutions. The response variable was the extent of oxidation, calculated based on the integrated EEM fluorescence spectra volume, as follows:

$$Extent\ of\ oxidation\ (\%) = \left(1 - \frac{V_t}{V_0}\right) \times 100 \qquad (2.1)$$

where V_t is the integrated EEM fluorescence spectra volume during the reaction, at a time t, and V_0 is the integrated EEM fluorescence spectra volume at the initial time of reaction (0 h). A $U_{12}(3^3)$ design was applied, as shown in Table 2.1, and three replicates of the design were performed in different days.

Table 2.1: The Uniform Design $U_{12}(3^3)$.

	Coded factors			**Uncoded factors**		
Run order	**x_1**	**x_2**	**x_3**	**[H_2O_2] (mM)**	**t (h)**	**pH**
1	1	2	3	0.5	4	7.0
2	2	3	1	2.5	7	4.0
3	3	3	2	5.0	7	5.6
4	3	1	2	5.0	2	5.6
5	2	1	3	2.5	2	7.0
6	3	2	1	5.0	4	4.0
7	1	1	2	0.5	2	5.6
8	2	1	1	2.5	2	4.0
9	2	3	3	2.5	7	7.0
10	3	2	3	5.0	4	7.0
11	1	3	2	0.5	7	5.6
12	1	2	1	0.5	4	4.0

Experimental data were analysed by best subsets regression analysis, in order to find the "best subsets", and, after their determination, regression analyses were executed for each regression model, to determine the significance level of each predictor variable. MINITAB (version 18) trial version was used for best subsets regression and for regression analyses. A model was obtained with a second order polynomial equation, which considers the interaction between the variables, and that can be expressed according to Equation 2.2:

$$Y = \beta_0 + \sum_{i=1}^{K} \beta_i x_1 + \sum_{i=1}^{K} \beta_{ii} x_{ii}^2 + \sum_{i \leq j}^{K} \sum_{j}^{K} \beta_{ij} x_i x_j + \varepsilon \qquad (2.2)$$

where i is the linear coefficient, j is the quadratic coefficient, β is the regression coefficient, k is the number of factors studied and optimized in the experiment and ε is the random error (Kasiri et al., 2008).

Python 3.7 was used for the identification of the optimal conditions, by defining the equation and the interval of values for each variable. The outcome of this procedure was a list of conditions (initial H_2O_2 concentration and reaction time) with expected percentages of extents of oxidation equal or higher than 99.5 %, according to the equation provided. From within the set of optimal conditions, an equilibrium between the concentration and the reaction time was searched, in order to have a minimum H_2O_2 concentration for a maximum reaction time of 4 h.

2.3 Confidence intervals for the model

Working-Hotelling confidence intervals, with a significance level of 95 %, were applied to the model and determined using Python 3.7, according to the equations presented ahead.

The X matrix is the matrix of parameter coefficients for each experiment and the column vectors Y and $\hat{Y}$ are the observed and predicted responses, respectively, being $\hat{Y}$ given by

$$\hat{Y} = X\hat{B} \tag{2.3}$$

where $\hat{B}$ is the matrix of parameter estimates, which can be obtained from (Deming and Morgan, 1987)

$$\hat{B} = (X^T X)^{-1}(X^T Y) \tag{2.4}$$

R is the matrix of residuals, which can be obtained from (Deming and Morgan, 1987)

$$R = Y - \hat{Y} \tag{2.5}$$

The R matrix multiplied by its transpose gives the sum of squares of residuals, SS_r (Deming and Morgan, 1987):

$$SS_r = R^T R \tag{2.6}$$

If a model does not present a serious lack of fit, then the variance of residuals, s_r^2, is given by:

$$s_r^2 = \frac{SS_r}{n-p} \tag{2.7}$$

where $n-p$ are the degrees of freedom of residuals, is a valid estimate of the population variance of residuals, σ_{pe}^2, and the equation

$$V = s_r^2 (X^T X)^{-1} \tag{2.8}$$

can be used to calculate the variance-covariance matrix (Deming and Morgan, 1987).

To set confidence intervals, one can use the variances of the parameter estimates (Deming and Morgan, 1987). Overall, the confidence interval for a parameter β, based on s_r^2, is given by:

$$b \pm \sqrt{F_{(1,n-p)} \times s_b^2} \tag{2.9}$$

where b is the estimated value of the true parameter β, s_b^2 is the variance from the diagonal of the variance-covariance matrix, and $F_{(1,n-p)}$ is the tabular value of F at a chosen level of confidence (Deming and Morgan, 1987).

The estimated variance of predicting a single new value of response at a given point in factor space, $s_{y_{10}}^2$, is equal to the sum of the purely experimental uncertainty variance, s_{pe}^2, and the variance of estimating the mean response at that point $s_{\hat{y}_{10}}^2$:

$$s_{y_{10}}^2 = s_{pe}^2 + s_{\hat{y}_{10}}^2 \tag{2.10}$$

where the subscript "0" is employed to denote that the factor combination of interest does not necessarily correspond to one of the experiments that was performed (Deming and Morgan, 1987). A 1 × f matrix X_0, which comprehends only one row, with columns corresponding to the columns of the X matrix, and whose elements correspond to the factor combination of interest is defined as (Deming and Morgan, 1987):

$$X_0 = [1 \quad x_{10} \quad x_{20} \quad x_{10}^2 \quad x_{20}^2 \quad x_{10}x_{20}] \tag{2.11}$$

The variance of predicting the mean response at a point in factor space is (Deming and Morgan, 1987):

$$s_{\hat{y}_{10}}^2 = s_{pe}^2[X_0(X^TX)^{-1}X_0^T] \tag{2.12}$$

Therefore,

$$s_{\hat{y}_{10}}^2 = s_{pe}^2 + s_{pe}^2[X_0(X^TX)^{-1}X_0^T] = s_{pe}^2\{1 + [X_0(X^TX)^{-1}X_0^T]\} \tag{2.13}$$

It is usual to use s_r^2 to estimate $s_{\hat{y}_{10}}^2$ when setting confidence intervals for response surfaces, to partly compensate for the possibility of a slight lack of fit between the model and the data (Deming and Morgan, 1987)

$$s_{\hat{y}_{10}}^2 = s_r^2\{1 + [X_0(X^TX)^{-1}X_0^T]\} \tag{2.14}$$

Through the modification of equation 2.14, the estimated variance of predicting the mean of m new values of response at a given point in factor space, $s_{\bar{y}_{10}}^2$, is (Deming and Morgan, 1987)

$$s_{\bar{y}_{10}}^2 = s_r^2\left\{\frac{1}{m} + [X_0(X^TX)^{-1}X_0^T]\right\} \tag{2.15}$$

Additionally, if m is large, Equation 2.15 can be simplified to (Deming and Morgan, 1987)

$$s_{\bar{y}_{10}}^2 = s_r^2[X_0(X^TX)^{-1}X_0^T] \tag{2.16}$$

It is possible to use equation 2.16 to obtain confidence intervals for predicting true mean responses (Deming and Morgan, 1987). This interval is given by

$$y_{10} = \hat{y}_{10} \pm \sqrt{W^2 \times s_{\hat{y}_{10}}^2} \tag{2.17}$$

where F was replaced by W^2, which is given by (Deming and Morgan, 1987):

$$W^2 = p \times F_{(p,n-p)} \tag{2.18}$$

where p is the number of parameters in the model (Deming and Morgan, 1987). Since

$$y_{10} = X_0\hat{B} \tag{2.19}$$

an equivalent expression for the confidence interval can be obtained by replacing Equations 2.16 and 2.19 in Equation 2.17 (Deming and Morgan, 1987):

$$\hat{y}_{10} = X_0\hat{B} \pm \sqrt{W^2 \times s_r^2[X_0(X^TX)^{-1}X_0^T]} \tag{2.20}$$

If X_0 is made to vary across the domain of factor space, Equation 2.20 can be used to plot the confidence intervals for predicting true mean values of response (Deming and Morgan, 1987).

2.3 Test of the UV/H_2O_2 process in rainwater samples

Two rainwater samples were collected at a sampling station located on the University of Aveiro campus', in the western part of the town of Aveiro, Portugal (40º38'N, 8º39'W; Figures 2.1 a and 2.1 b), on 5 and 6 April 2019 (samples 1 and 2, respectively).

Rainwater sampling was carried out 70 cm above the ground, through glass funnels (30 cm diameter) into glass bottles (5 L), placed inside PVC (polyvinyl chloride) opaque tubes, to ensure protection from direct sunlight and to minimize changes due to photochemical reactions (Santos et al., 2014). As shown in Figure 2.1 c, four collectors of rainwater were used simultaneously. These collectors were left out open at 10 h of local hour, during a period of 24 h, and both wet and dry depositions were collected.

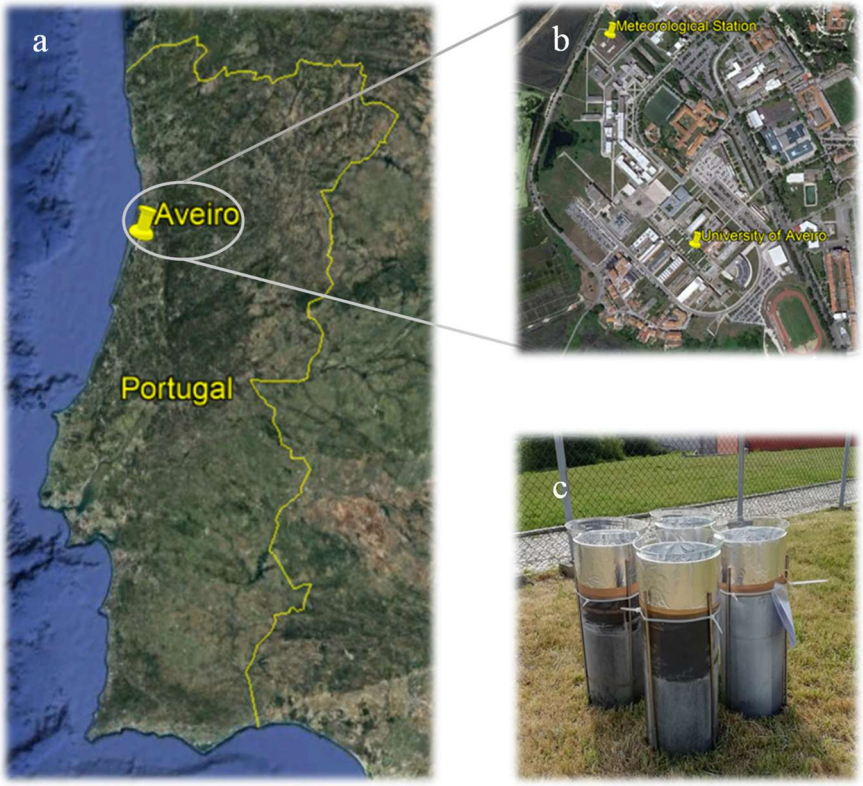

Figure 2.2: a) Schematic map of Portugal; **b)** Campus of the University of Aveiro; **c)** Rainwater collectors at the sampling station.

After collection, the samples were divided into two aliquots. One of the aliquots was used for the immediate measurement of the pH and electrical conductivity (σ) (Table 2.2). A second aliquot was filtered through hydrophilic PVDF (polyvinylidene fluoride) Millipore membrane filters with 0.45 µm of pore size, and a fraction of this volume was used for the immediate optical analysis (UV-Vis and molecular fluorescence spectroscopy). The remaining volume was frozen, for posterior analysis.

In Table 2.2, the volume collected, the pH and electrical conductivity, for each sample, are presented.

Table 2.2: Volume (mL), pH and σ (µS cm^{-1}) for each collected sample.

	Sample 1	**Sample 2**
Collected Volume (mL)	6100	2760
pH	5.2	5.4
σ (µS cm^{-1})	19	63

Experiments with the two rainwater samples, at their natural pH, were performed in a similar way to what was described above for model solutions, in order to test the influence of the matrix on the oxidation of the mixture of contaminants by the UV/H_2O_2 process. For such, samples were spiked with the contaminants (benzoic acid, 3,5-dihydrozybenzoic acid, and syringic acid, each one with a concentration of 0.02 mM), and H_2O_2 was added (to obtain a concentration of 5.0 mM) to initiate the reaction, and oxidation was evaluated for the reaction times of 0 h, 2 h and 4 h. Control experiments were also performed in similar way for samples, for samples spiked with H_2O_2, and for samples spiked with the mixture of contaminants and without H_2O_2. Additionally, experiments at the optimum conditions (3.1 mM of H_2O_2 and 4 h of reaction time) were carried out for both samples spiked with the mixture of contaminants, and two replicates were made.

2.5 Optical analysis

UV-Vis spectra, in the range of 200-500 nm, were recorded on a Shimadzu (Dusseldorf, Germany) Model UV 210PC spectrophotometer using quartz cells of 1 cm path lengths for the oxidation experiments, and of 10 cm path lengths for the rainwater samples. Ultrapure water was used as reference, to obtain the baseline.

The molecular fluorescence spectra were obtained using a Jasco FP-6500 spectrophotometer with a xenon lamp as the source of radiation and using 1 cm quartz cells. Synchronous spectra with $\Delta\lambda$ of 60 nm (Santos et al., 2009) were acquired using excitation wavelengths (λ_{exc}) from 280 nm to 560 nm with sequential increments of 5 nm. The spectra were recorded at a scan speed of 500 nm min^{-1}, using 5 nm band widths on both the excitation and emission monochromators. Excitation-emission matrix (EEM) fluorescence spectra were obtained by concatenating emission spectra measured every 5 nm from 230 nm to 500 nm using excitation wavelengths from 220 nm to 450 nm, increasing at 10 nm intervals. The spectra were recorded at a scan speed of 500 nm min^{-1}, using 5 nm band widths on both the excitation and emission monochromators. For each day of experimental work, the fluorescence blank spectrum (ultrapure water) was subtracted from the solutions spectra.

Chapter 3

Results and discussion

3.1 Degradation of contaminants by the UV/H_2O_2 oxidation process

The degradation of a mixture of contaminants, containing benzoic acid, 3,5-dihydroxybenzoic acid and syringic acid (BA, DHBA and SA, respectively) by the UV/H_2O_2 oxidation process was evaluated in water model solutions. Nevertheless, before the oxidation of the mixture, the oxidation of the individual compounds was also performed as control, in order to predict their behavior in the oxidation of the mixture. Figure 3.1 shows the UV–Vis spectra recorded during the oxidation of BA, DHBA, SA and of the mixture, by UV/H_2O_2, at a pH value of 5.6 (neutral for atmospheric water) and with an initial H_2O_2 concentration of 0.5 mM.

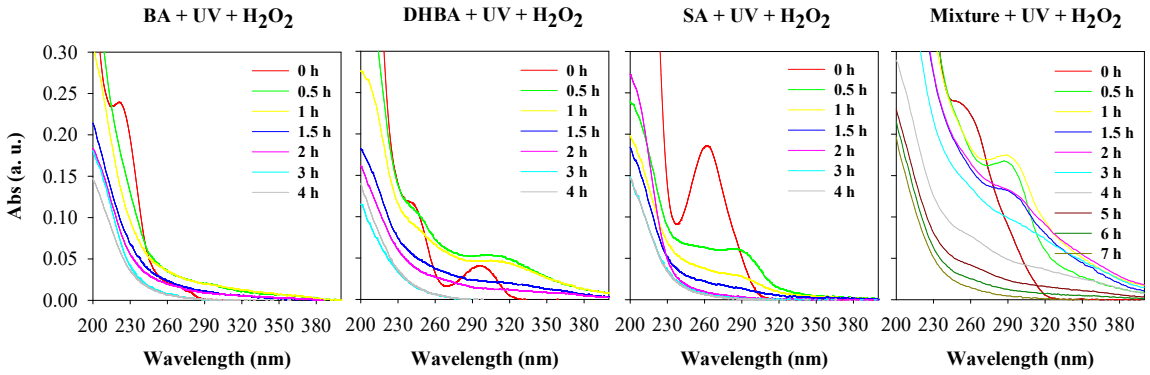

Figure 3.1: Absorbance spectra (average spectra) of benzoic acid (BA), 3,5-dihydroxybenzoic acid (DHBA), syringic acid (SA) and of the mixture of these three acids (mixture) during the oxidation by UV/H_2O_2, with $[H_2O_2]_0$ of 0.5 mM and at pH 5.6.

As shown in Figure 3.1, at the initial time (0 h), BA presents a principal absorption band at 222 nm, and a secondary band around 270 nm. The locations of these absorption bands are due to the π-π* electronic transitions, associated with the benzene ring and with the carboxylic group (Williams & Fleming, 1989), and are similar to those reported by Santos et al. (2015; 2019). On its turn, the spectrum of 0 h, for DHBA, has a principal absorption band located at 242 nm, and a secondary absorption band at 298 nm, while the spectrum of 0 h, for SA, has a principal absorption band at 261 nm, and a secondary band that is completely submerged in the principal band (Santos et al., 2016a). Considering that the molecular structure of BA is the base unit of DHBA and SA, the differences in the location of the absorption bands, when compared to BA, are due to the substitution of the benzene ring by two hydroxyl groups (at meta positions) in the case of DHBA, and by one hydroxyl group (at para position) and two methoxy groups (at meta positions) in the case of SA (Williams & Fleming, 1989). The wavelength of the principal absorption bands increases with the increase of the substitution to the benzene ring in the following order: BA<DHBA<SA. Additionally, with more substitution, principal bands move to longer wavelengths faster than secondary bands, and may overtake them (Williams & Fleming, 1989), which is evident in the spectrum of SA, where the secondary band is submerged in the principal band. The location of the absorption bands for DHBA and SA, at the initial time, is similar to those described by Santos & Duarte (2015) and Santos et al. (2016b), respectively. In what concerns the spectrum of the mixture of contaminants, at 0 h, a single absorption band can be noticed, and it is located at 252 nm, resulting from the overlapping of the individual bands of each compound.

With the course of the oxidation of the individual compounds and of the mixture of compounds by UV/H_2O_2, the initial absorption bands (at 0 h) disappear and originate other bands, located at different wavelengths. These findings suggest the occurrence of chemical reactions, and that the degradation of the compounds is occurring with the course of time.

In the case of BA, as it can be verified in Figure 3.1, in the spectrum of 0.5 h, both absorption bands present at 0 h, can no longer be identified. The overall absorbance of the spectra decreases with time, and, after 3 h of reaction, no notable differences in the UV-Vis spectra can be observed. In turn, the spectra of DHBA reveal that the absorption band located at 242 nm is less intense after 0.5 h of reaction, and that it cannot be recognized after 1 h of reaction. Moreover, the absorption band located at 298 nm displaces to 310 nm at 0.5 h of

reaction, and its absorbance decreases from 0.5 h to 1 h. After 1.5 h of reaction, both absorption bands disappear, and the overall absorbance of the spectra decreases, until 3 h, time after which there are no notable differences in the UV-Vis spectra. On the other hand, the absorption band of SA decreases from 0 h to 0.5 h, and an absorption band appears at a wavelength of 290 nm. After 1.5 h, no absorption bands can be identified, and the overall absorbance of the spectra continues to decrease with time, until 3 h, from when no substantial differences in the spectra can be perceived. The band of absorption of the mixture of the three acids, located at 252 nm, disappears after 0.5 h of reaction, and a new band appears at a wavelength of about 290 nm, which, after 3 h of reaction, also disappears. The overall absorbance of the spectra continues to decrease until the end of the reaction (7 h).

In order to evaluate the degradation of the above-mentioned contaminants and of the mixture, the oxidation reactions were accompanied by molecular fluorescence spectroscopy. Figure 3.2 shows the synchronous fluorescence spectra of BA, DHBA and SA at an initial pH of 5.6, before and after the oxidation by UV/H_2O_2, with an initial concentration of H_2O_2 of 0.5 mM.

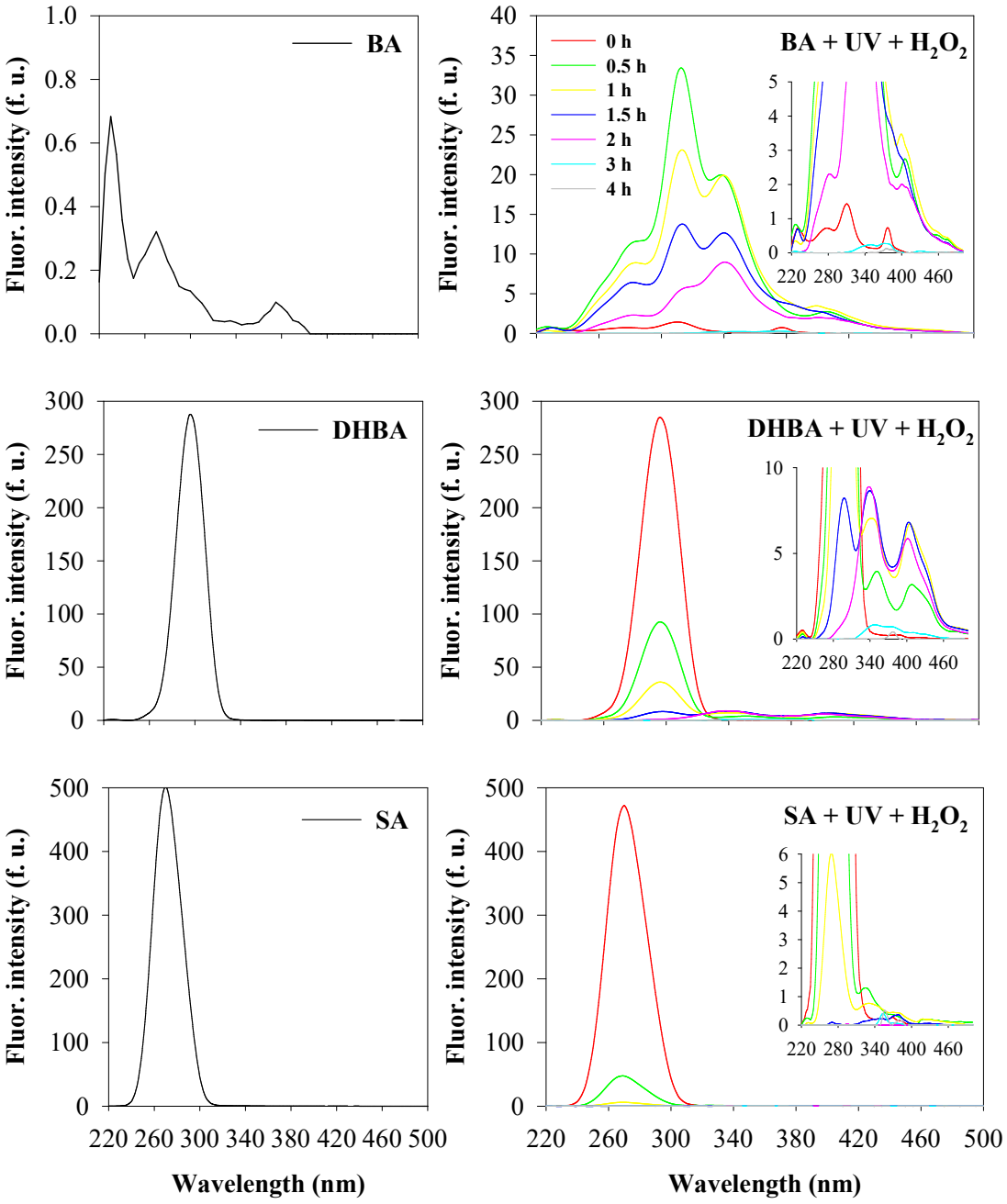

Figure 3.2: Synchronous fluorescence spectra (Δλ = 60 nm) of benzoic acid (BA), of 3,5-dihydroxybenzoic acid (DHBA) and of syringic acid (SA), at pH 5.6 (left), and of BA, DHBA and SA, during the oxidation by UV/H_2O_2, with $[H_2O_2]_0$ of 0.5 mM and at pH 5.6 (right). The legend contained inside the window of the oxidation of BA by UV/H_2O_2 is the same for all oxidation spectra.

To confirm the partial or total degradation of the compounds by UV/H_2O_2 in water, EEM fluorescence spectroscopy analyses were also performed throughout the oxidation process. Figure 3.3 shows the spectra obtained before and after the oxidation of BA, DHBA and SA by UV/H_2O_2, at a pH of 5.6 and with an initial H_2O_2 concentration of 0.5 mM.

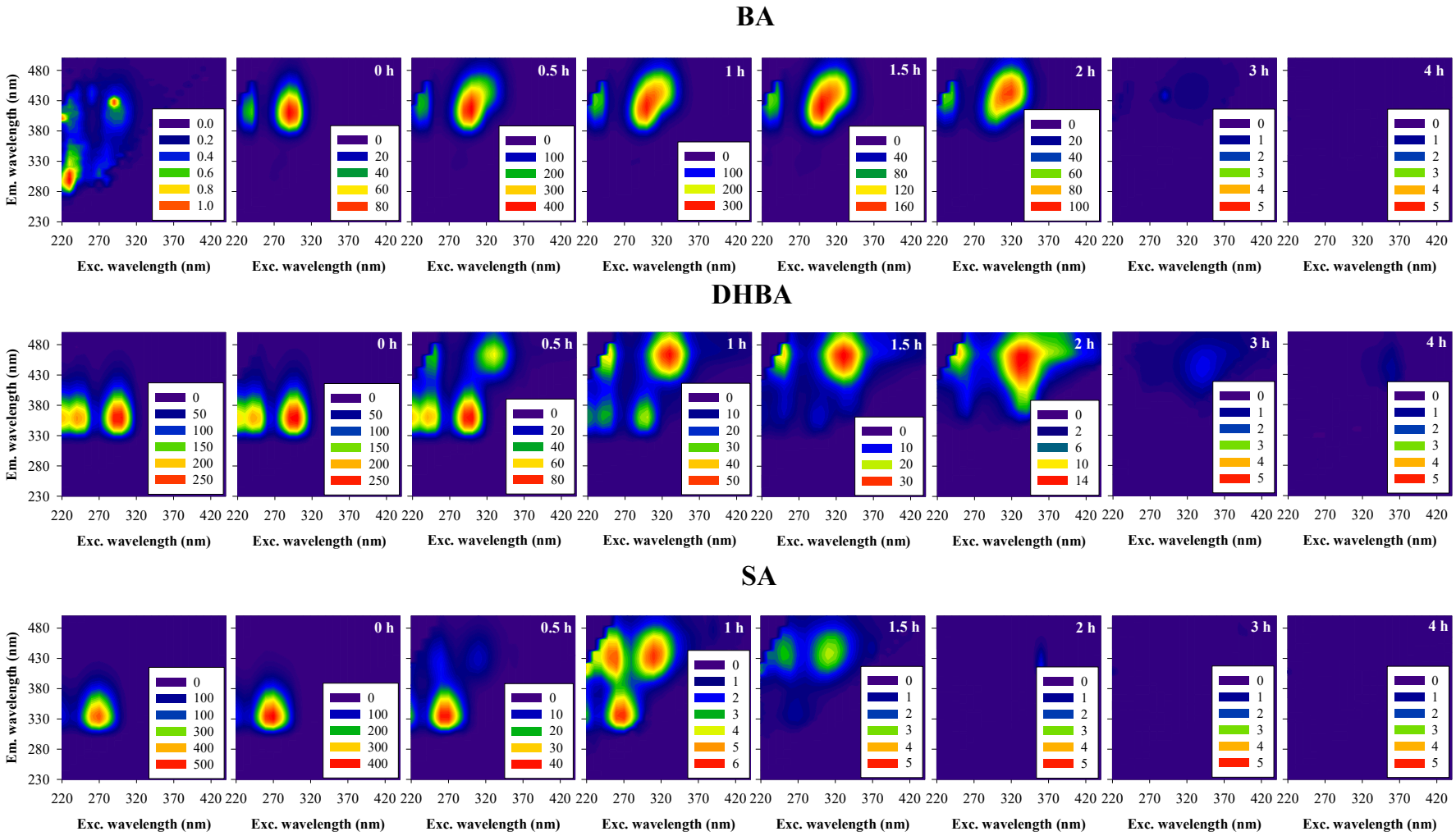

Figure 3.3: Excitation-emission matrix (EEM) fluorescence spectra of BA, DHBA and SA, before (first spectrum of each row) and during the oxidation by UV/H_2O_2, at pH 5.6, $[H_2O_2]_0$ of 0.5 mM, and for the oxidation times of: 0 h, 0.5 h, 1 h, 1.5 h, 2 h, 3 h and 4 h.

The synchronous fluorescence spectrum of BA before the oxidation (Figure 3.2) indicates the presence of three fluorescent bands, with maximums located at 230 nm, 270 nm and 378 nm of excitation wavelength. While observing the synchronous fluorescence spectrum of BA, obtained immediately after the addition of H_2O_2 (0 h), the presence of the fluorescent band at 230 nm is still notable. However, the band at 270 nm slightly displaces to 280 nm, and the intensity of the band at 378 nm increases. Furthermore, a new fluorescent band appears, at about 310 nm. These changes to the spectrum are the result of the addition of H_2O_2 to the solution, conducting to the presence of hydroxyl radicals and simultaneous hydroxylation of BA, which was observed at the moment of analysis (because 0 h is the time after the addition of H_2O_2 and the reading time). After 0.5 h of reaction, the overall intensity of the spectrum increases, and, in addition, new fluorescent bands appear at about 340 nm and 410 nm. This is in accordance with the results of a study by Santos et al. (2016b), where, during the Fenton-like oxidation of BA, new bands at longer excitation wavelengths appeared, suggesting that BA was hydroxylated. Nevertheless, after 1 h of reaction, the overall intensity starts to diminish, and, after 3 h, no notable differences in the spectra can be identified.

According to Figure 3.3, the EEM fluorescence spectrum of BA before the oxidation, presents three fluorescent bands: one located at 220 nm of excitation and 400 nm of emission wavelength; a second one located at 230 nm of excitation and 300 nm of emission wavelength, which can also be seen in the synchronous fluorescence spectra of BA; and a third band, located at 290 nm of excitation and 430 nm of emission wavelength. Immediately after the addition of H_2O_2 (0 h), the intensity of the bands increases and only two bands can be observed: one located at 290 nm of excitation and 430 nm of emission wavelength, which is the band with the highest intensity; and another band located at 240 nm of excitation and 420 nm of emission wavelength. After 0.5 h, a new band, submerged in the principal band (290 nm of excitation and 430 nm of emission), starts to appear, and these two bands remain attached throughout the reaction, moving to higher excitation wavelengths during the process (318 nm of excitation and 440 nm of emission wavelengths). Moreover, the intensity of the bands only starts to decrease after 1 h of reaction, and, after 4 h, no fluorescent bands can be seen, suggesting that no chromophoric compounds remain in solution. As mentioned before, the spectra of the oxidation of BA, either the synchronous, as the EEM spectra, suggest the formation of new compounds during the process through the appearance of new

fluorescent bands at longer excitation wavelengths, not present in the spectra of BA before the oxidation. Deng et al. (2006) identified 2-hydroxybenzoic acid, 3-hydroxybenzoic acid, 4-hydroxybenzoic acid and 3,4-dihydroxybenzoic acid as products of the oxidation of BA by radiation at 254 nm, the same radiation wavelength used in this work. The authors suggest that hydroxyl radicals ($OH^{\cdot}$) and/or hydroperoxyl radicals ($HO_2^{\cdot}$) may attack the ortho, meta and para positions of benzoate ions ($C_6H_5COO^-$), originating mono-hydroxybenzoic acids and di-hydroxybenzoic acids. Furthermore, a Fenton-like oxidation study by Santos et al. (2016a), also with BA, identified 2-hydroxybenzoic, 3-hydroxybenzoic, 4-hydroxybenzoic, 2,3-dihydroxybenzoic, 2,5-dihydroxybenzoic, 2,6-dihydroxybenzoic, and 3,4-dihydroxybenzoic acids, as intermediate compounds of the oxidation of BA. Given the similarities between the mentioned studies and the present work, the compounds identified by these authors could be the same intermediate compounds formed during the oxidation of BA in this study.

Regarding DHBA, the synchronous spectrum before the oxidation shows a single fluorescent band with a maximum located at 298 nm of excitation wavelength, which is also present, with a similar intensity, in the spectrum at the initial time of oxidation (0 h). Additionally, the location of this band is similar to the one reported by Santos & Duarte (2015) for the same compound. After 0.5 h of reaction, the intensity of this fluorescent band diminishes, and two new fluorescent bands appear, one at an excitation wavelength of 350 nm and the other at 405 nm. After 1 h of reaction, the band located at 350 nm moves to 340 nm, but the intensity of this band, and of the one located at 405 nm remains unchanged, unlike the main fluorescent band, whose intensity decreases. Furthermore, after 2 h of reaction, the band located at 298 nm vanishes, and the intensity of the fluorescent band located at 405 nm starts to decrease. After 3 h, the overall spectrum intensity is very low, suggesting that there are no chromophoric compounds in the solution after 3 h of reaction. The synchronous fluorescence spectra of the oxidation of DHBA show some similarities when compared to the spectra of the oxidation of BA, namely in the formation of the fluorescence bands located at longer excitation wavelengths, near 340 nm and 405 nm, which appear during the oxidation of both compounds. Possibly, during the oxidation of both compounds, similar intermediate compounds are formed, as they fluoresce in the same wavelengths.

Similarly, the synchronous spectra and the EEM spectra of DHBA before the oxidation reaction and at 0 h are very much alike. Both present a fluorescent band located at 240 nm of excitation wavelength and 360 nm of emission wavelength, and another fluorescent band at 300 nm of excitation wavelength and 360 nm of emission wavelength. This last band has a similar location to one of the bands present in the synchronous spectra (298 nm). After 0.5 h of reaction, the intensity of these bands decreases, and new bands appear: one at 250 nm of excitation wavelength and 460 nm of emission wavelength, and other at about 330 nm of excitation wavelength and 455 nm of emission wavelength. The fluorescence intensity continues to decrease with the reaction time, and, after 3 h of oxidation, the only band that can be seen is the one located at 330 nm of excitation and 455 nm of emission wavelength. After 4 h, no fluorescence bands can be clearly seen in the spectrum, suggesting that the chromophoric compounds were completely degraded. Like in the case of BA, during the oxidation of DHBA, the formation of new compounds throughout the process is suggested by the synchronous and by the EEM fluorescence spectra, through the appearance of new fluorescent bands. Some of these compounds could be 2,4,6-trihydroxybenzoic acid, 3,4,5-trihydroxybenzoic acid and tetrahydroxybenzene, which were intermediate compounds identified during the Fenton-like oxidation of DHBA by Santos et al. (2016a).

On its turn, the synchronous spectrum of SA before oxidation presents a single fluorescent band at 270 nm of excitation wavelength, which is also present in the spectrum of the initial time of oxidation (0 h), but with a slightly lower intensity. Furthermore, the location of this band is the same as the reported by Santos et al. (2016b) for the same compound. From 0 h to 0.5 h, its intensity decreases significantly, and a new fluorescent band appears at 325 nm, suggesting the formation of a new chromophoric compound. The overall fluorescence intensity of the spectra decreases with the reaction time, and after 3 h of reaction, there are no chromophoric compounds lasting in the solution.

Additional information, during the oxidation of SA by UV/H_2O_2, is given by the EEM spectra present in Figure 3.3. The EEM spectrum of SA before the oxidation presents only one fluorescent band, located at 270 nm of excitation wavelength and 335 nm of emission wavelength, which coincides with the location of the fluorescence band present in its synchronous spectrum. After adding H_2O_2 to the solution (0 h), this is the only band present in the spectrum, but with a lower intensity, which suggests that this compound starts

to degrade right after the addition of H_2O_2. In the spectrum of 0.5 h, new bands start to appear, and, in the spectrum of 1 h, two new fluorescent bands can be identified, one at 260 nm of excitation wavelength and 430 nm of emission wavelength, and other at 310 nm of excitation wavelength and 435 nm of emission wavelength. After 1.5 h of reaction, only the newly formed bands can be seen. The spectrum of 3 h does not present any fluorescence, suggesting that all chromophoric compounds were degraded. Santos et al. (2016b) showed that, the oxidation of SA by Fenton-like reaction in the absence of light, originates fluorescent bands at the same locations as those obtained in this study by UV/H_2O_2, which suggests the formation of the same compounds. Santos el al. (2016b) identified one of those intermediate compounds as being 1,4-dihydroxy-2,6-dimethoxybenzene, which could be also formed during the oxidation of SA in this study, given that the same fluorescent bands are present in both studies.

Overall, when the three organic acids were oxidized by UV/H_2O_2, new fluorescent bands appeared at longer excitation wavelengths. These fluorescent bands may have possibly resulted from the increase of π-electron systems and of substitution of benzene rings by electron-donator groups, such as hydroxyl groups (Santos & Duarte, 2019). This is a consequence of the presence of $OH^{\cdot}$ in solution, formed due to the photolysis of H_2O_2, which attack and degrade the organic compounds.

The synchronous fluorescence spectra of the mixture of the three compounds obtained before and during the oxidation of the mixture by UV/H_2O_2, with an initial H_2O_2 concentration of 0.5 mM, and at an initial pH of 5.6, are present in Figure 3.4.

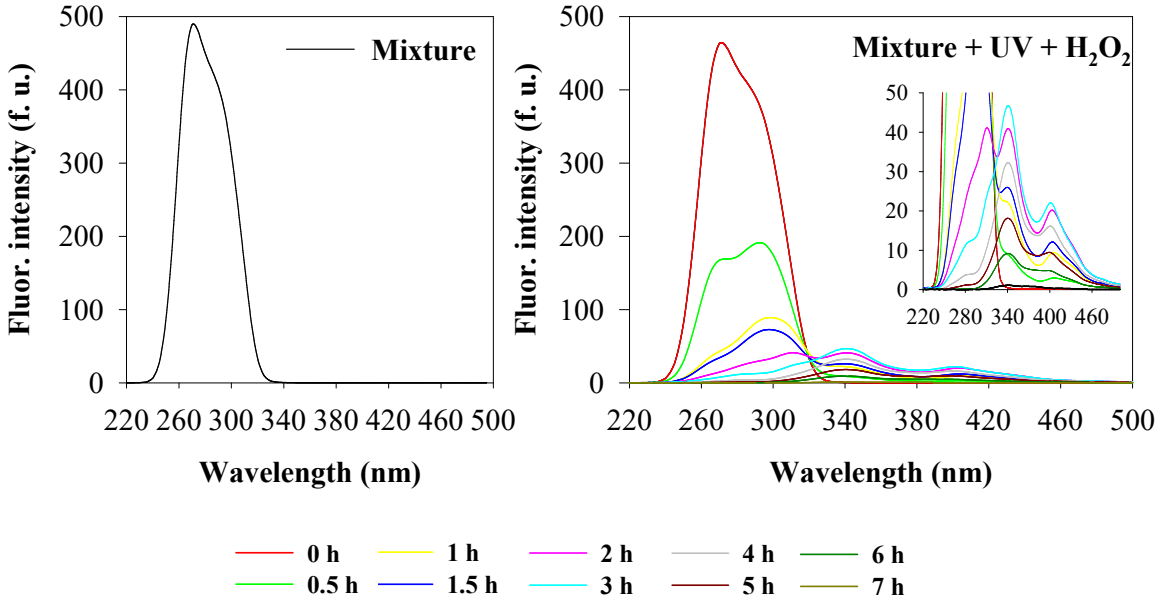

Figure 3.4: Synchronous fluorescence spectra ($\Delta\lambda$ = 60 nm) of the mixture of the three acids (BA, DHBA and SA), at pH 5.6 (left) and of the mixture of acids during the oxidation by UV/H_2O_2, with $[H_2O_2]_0$ of 0.5 mM, at pH 5.6 (right).

EEM fluorescence spectroscopy analyses were also employed throughout the UV/H_2O_2 oxidation process of the mixture of the three contaminants, with an initial H_2O_2 concentration of 0.5 mM, and at an initial pH of 5.6. The spectra obtained are shown in Figure 3.5.

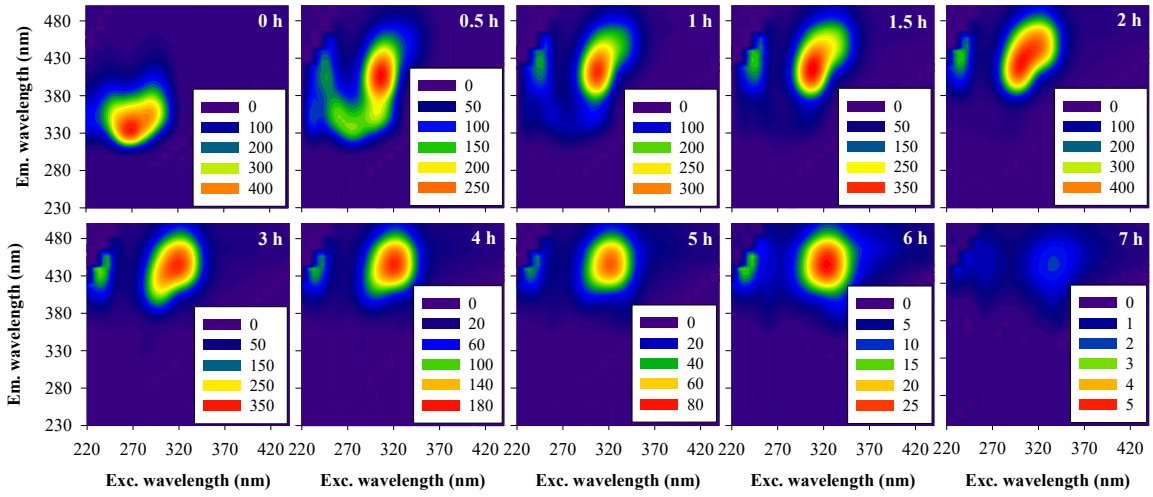

Figure 3.5: Excitation-emission matrix (EEM) fluorescence spectra of the mixture of the three contaminants during the oxidation with UV/H_2O_2, at pH 5.6, $[H_2O_2]_0$ of 0.5 mM, and for the oxidation times of: 0 h, 0.5 h, 1 h, 1.5 h, 2 h, 3 h, 4 h, 5 h, 6 h and 7 h.

The synchronous spectrum of the contaminants' mixture presents two fluorescence bands, one is located at 270 nm, and the other is submerged in this one, possibly situated at 300 nm, which is the location of the fluorescent band of DHBA. The first band is situated at the same wavelength at which the only fluorescent band in SA is located, as shown in Figure 3.2. At 0 h, after the addition of H_2O_2 to the solution, the spectrum decreases its intensity, which means that the compounds are being oxidized. This can be seen right after 0.5 h of reaction, as the intensity of the bands significantly decreased compared to the intensities of the spectrum of 0 h. As the reaction continues, the formation of new compounds is suggested by the appearance of new bands. These bands, similar to what happened with the oxidation with the individual compounds, are located at higher excitation wavelengths, namely at 340 nm and 405 nm, which suggests that compounds with higher levels of complexity are being formed. After 1 h of oxidation, the band previously at 300 nm moves to higher excitation wavelengths (310 nm), before disappearing (3 h). With the course of reaction, the bands tend to decrease their intensities, and within 7 h, the bands at 340 nm and 405 nm present very low intensities, suggesting that a low content of chromophoric compounds remains in solution. The spectra of the oxidation of the mixture present some similarities with the spectra of the oxidation of BA and DHBA, since new fluorescent bands appeared, namely at 340 nm and 405 nm.

The same bands which appear in the synchronous spectrum of the mixture before the oxidation, are also present in the EEM spectrum of the mixture before (see Figure 3.6, reaction time of 0 h) and at 0 h of oxidation. One band is located at 270 nm of excitation and 335 nm of emission wavelength and the other is submerged in this one. After 0.5 h of oxidation, the band located at 270 nm of excitation and 335 of emission wavelength begins to disappear, and two new bands start to form. At this point in time, it is also possible to see a fluorescent trace linking these two bands, highlighting that the initial chromophoric compounds are in the process of transformation. This fluorescent trace starts to disappear in the spectrum of 1 h, and the new bands can now be clearly seen: one is located at 240 nm of excitation and 420 nm of emission, and the other one is located at 300 nm of excitation and 415 nm of emission. A fluorescent band, located at a similar wavelength of the band located at 240 nm of excitation and 420 nm of emission wavelengths, is present in the spectrum of the oxidation of BA, suggesting that similar compounds could be forming during the oxidation of the mixture and of BA. This resemblance with BA occurs because its oxidation

is slower than the oxidation of the other two organic acids. Moreover, the fluorescent bands in the BA oxidation spectra have a higher intensity than the bands present in the spectra of the other acids, possibly overlapping the bands of the other acids, when present as a mixture. In the spectra of the mixture, the main fluorescent band (300 nm of excitation and 415 nm of emission wavelength), moves to longer excitation wavelengths during the reaction, and has a similar behavior and a similar location as the main fluorescence band during the oxidation of BA. Furthermore, like in the case of BA, a fluorescent band seems to be submerged in this band during the oxidation of the mixture. Once more, these findings suggest that the same compounds could be formed during the oxidation of BA and of the mixture. Only after 3 h of reaction does the intensity of the bands, present in the spectra of the mixture, start to decrease. At this point in time, the spectra of the individual compounds suggest that the chromophoric compounds were almost completely degraded, which did not happen for the mixture. This could be explained by the fact that the compounds are in a mixture, and not individually. Thus, there is a higher content of compounds in solution for the same amount of hydroxyl radicals. On this scenario, H_2O_2 could be acting as the limiting reagent, but the occurrence of parallel reaction, or competition for the chemical oxidants and/or UV, could also cause the reaction to be slower (Boris et al., 2015; Santos et al., 2019). In fact, besides the oxidation of the mixture of compounds by the action of hydroxyl radical, the oxidation also occurs in the presence of only UV light, as it can be seen in Figure 3.6 and in Figure B.1 (Appendix B), which highlight the occurrence of parallel reactions by the action of the UV ligth. In the spectrum of the mixture, correspondent to 4 h of reaction, the band located at 300 nm of excitation and 415 nm of emission moves to 320 nm of excitation and 445 nm of emission, which are wavelengths similar to wavelengths at which fluorescent bands during the oxidation of the three acids are located. Once more, these observations could mean that, during the oxidation of the acids and of the mixture, similar compounds could be formed. As mentioned before, during the oxidation, the fluorescence bands move to higher excitation wavelengths, suggesting that the compounds formed have higher complexity than the original compounds, and present higher substitution of benzene rings by electron-donator groups, such as hydroxyl (Santos & Duarte, 2015). With the course of reaction, the intensity of the bands present in the spectra of the mixture continues to decrease, and, at the end of 7 h of reaction, almost all chromophoric compounds seem to be degraded.

All these results suggest that, during the oxidation by UV/H_2O_2, the three acids tested, and the mixture of the acids, are oxidized throughout time. However, while within 4 h the three acid compounds (when alone) seem to be completely degraded, at least in what regards to chromophoric compounds, the mixture of the three acids requires 7 h of reaction to achieve similar outcomes.

Figure 3.6 shows the EEM fluorescence spectra of the oxidation of the mixture of contaminants by UV light, at pH 5.6 for 0 h, 2 h, 4 h and 7 h, performed as control.

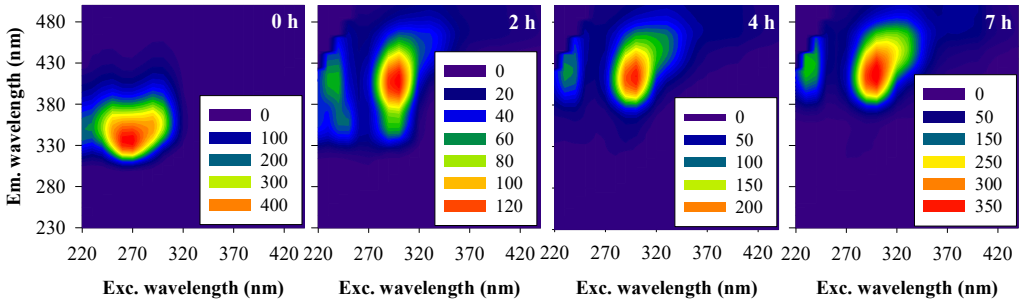

Figure 3.6: Excitation-emission matrix (EEM) fluorescence spectra of the mixture of the three contaminants during the oxidation with UV, at pH 5.6 and for the oxidation times of 0 h, 2 h, 4 h and 7 h.

From the observation of the EEM spectrum of the mixture at 0 h, it can be asserted that it presents a fluorescent band located at 270 nm of excitation wavelength and 335 nm of emission wavelength, and another band submerged in this one. This was also verified in the spectrum of 0 h in the oxidation of the mixture by the UV/H_2O_2 process. Overall, the oxidation of the mixture by UV light as some similarities with the oxidation of the mixture by UV/H_2O_2. For instance, the same fluorescence bands are present in both processes, and, in the oxidation by both processes, the intensity of the fluorescence bands decreases, to later increase. However, in the case of the oxidation by UV/H_2O_2, the intensity decreases from 0 h to 0.5 h of reaction, and increases from 0.5 h to 2 h, to then decrease until almost no chromophoric compounds are present in solution. On the other hand, regarding the oxidation by UV, the intensity of the bands decreases from 0 h to 2 h, and increases from 2 h until, at least, 7 h. In terms of fluorescence intensity, the spectra of 7 h, from the oxidation by UV, is similar to the spectra of 1.5 h from the oxidation by UV/H_2O_2, which suggests that the oxidation by UV is slower than the oxidation by UV/H_2O_2. These findings reveal that UV light is able to oxidize the mixture to some extent, but that the oxidation by UV/H_2O_2 is more

efficient due to the action of H_2O_2 in solution, which provides hydroxyl radicals that attack the compounds in solution.

3.2 Effect of H_2O_2 concentration on the oxidation of the mixture of contaminants

In order to verify the effect of H_2O_2 concentration on the oxidation of the mixture of contaminants by the UV/H_2O_2 process, and to make the degradation process faster, three concentrations of H_2O_2 were tested, namely: 0.5 mM, 2.5 mM and 5.0 mM. Figure 3.7 presents the UV-Vis spectra during the oxidation of the mixture at a pH value of 5.6, up to 4 h, using initial H_2O_2 concentrations of 0.5 mM, 2.5 mM and 5.0 mM.

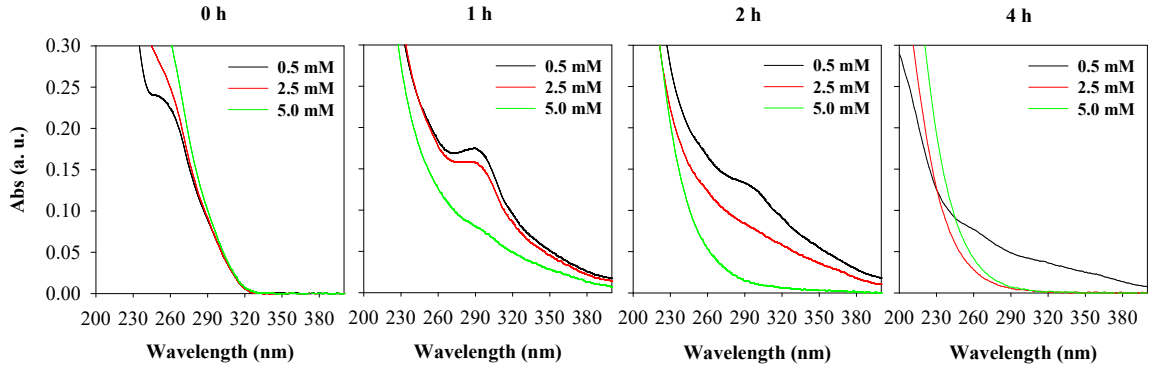

Figure 3.7: UV-Vis spectra during the oxidation of the mixture of contaminants by UV/H_2O_2, for: 0 h, 1 h, 2 h and 4 h, at pH 5.6, and $[H_2O_2]_0$ of 0.5 mM, 2.5 mM and 5.0 mM.

This figure reveals that, with higher H_2O_2 concentrations, higher oxidation rates are obtained. At 0 h, higher concentrations of H_2O_2 cause higher absorbances, because H_2O_2 contributes to the absorbance of the spectra. After the oxidation starts, higher concentrations of H_2O_2 conduct to lower absorbances, since there are more hydroxyl radicals present in solution to react with the compounds and to degrade them. However, after 4 h, similar absorbances were obtained for 2.5 mM and 5.0 mM, which suggests that a similar stage of oxidation was obtained.

Figure 3.8 shows the synchronous fluorescence spectra obtained during the oxidation of the mixture of contaminants by the UV/H_2O_2 process, with H_2O_2 concentrations of 0.5 mM, 2.5 mM and 5.0 mM, at a pH of 5.6.

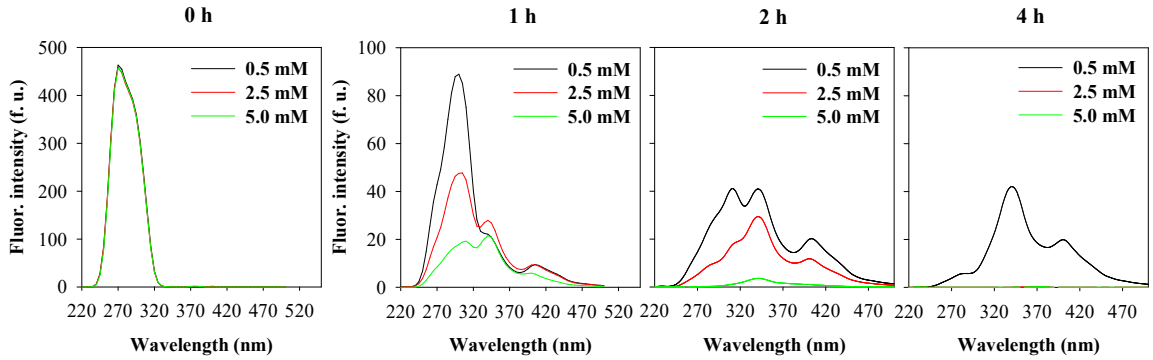

Figure 3.8: Synchronous fluorescence spectra (Δλ = 60 nm) during the oxidation of the mixture of contaminants by the UV/H_2O_2 process after 0 h, 1 h, 2 h and 4 h, at pH 5.6, $[H_2O_2]_0$ of 0.5 mM, 2.5 mM and 5.0 mM.

EEM fluorescence spectra, obtained during the oxidation of the mixture of contaminants by the UV/H_2O_2 process, with initial H_2O_2 concentrations of 0.5 mM, 2.5 mM and 5.0 mM, at a pH of 5.6, were also obtained and can be observed in Figure 3.9.

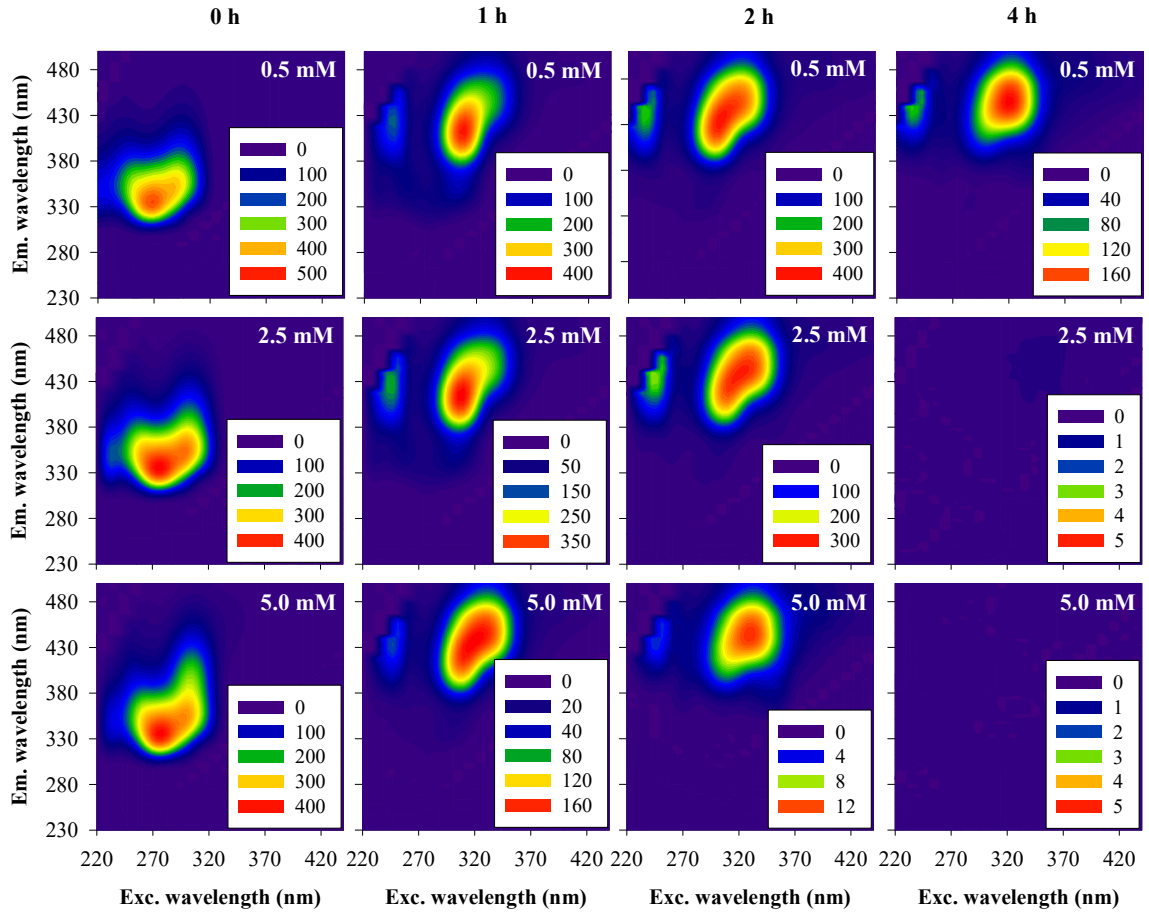

Figure 3.9: Excitation-emission matrix (EEM) fluorescence spectra during oxidation of the mixture of contaminants by UV/H_2O_2 after 0 h, 1 h, 2 h, and 4 h, at pH 5.6, $[H_2O_2]_0$ of 0.5 mM (upper row), 2.5 mM (middle row) and 5.0 mM (bottom row).

From the observation of the synchronous spectra, it can be said that the same conclusions drawn for the UV-Vis spectra apply to it, where, at 0 h, the three spectra have the same intensity, but, after the reaction starts, the higher the H_2O_2 concentration cause lower fluorescence intensity, and, thus, less compounds remain in solution. With higher H_2O_2 concentrations, higher oxidation rates are achieved. From the analysis of the spectra, it is clear that a concentration of 0.5 mM of H_2O_2 is not enough to degrade all chromophoric compounds in solution within 4 h, as there are still fluorescent bands present in the spectrum. Given that a concentration of H_2O_2 of 0.5 mM is in the same order of magnitude as the environmental H_2O_2 concentration (Vione et al., 2006), the H_2O_2 that exists naturally, is not enough to degrade the mixture of contaminants in 4 h.

Through the analysis of the EEM fluorescence spectra, it can be clearly seen that higher H_2O_2 concentrations lead to higher oxidation rates. When using a concentration of H_2O_2 of 0.5 mM, there are still chromophoric compounds in solution at 4 h of reaction, while, for 2.5 mM and 5.0 mM of H_2O_2, no chromophoric compounds remain. These findings reveal that the concentration of H_2O_2 has a major role in the time of oxidation of the mixture, since, when higher concentrations are used, there are more hydroxyl radicals available in solution to oxidize the compounds. As discussed in the preceding section, to obtain the almost total degradation of the mixture of contaminants using 0.5 mM of H_2O_2, 7 h of reaction were needed. However, when 2.5 mM and 5.0 mM of H_2O_2 are used, only 4 h of reaction are needed to degrade all the chromophoric content in solution. This highlights that, if one wishes a higher oxidation rate of the mixture of contaminants, a higher H_2O_2 concentration should be used.

3.3 Effect of pH on the oxidation of the mixture of contaminants

In order to evaluate the influence of the pH in the oxidation of the mixture of contaminants by UV/H_2O_2, three different pH's were tested, namely: 4.0, 5.6 and 7.0. The concentration of H_2O_2 used for the oxidation was 5.0 mM, and, thus, the maximum reaction time was set for 4 h, which is the time needed to completely degrade de compounds with this concentration. Figure 3.10 presents the UV-Vis spectra during the oxidation of the mixture of contaminants by UV/H_2O_2, for 0 h, 1 h, 2 h, 3 h and 4 h, at pH 4.0, 5.6 and 7.0.

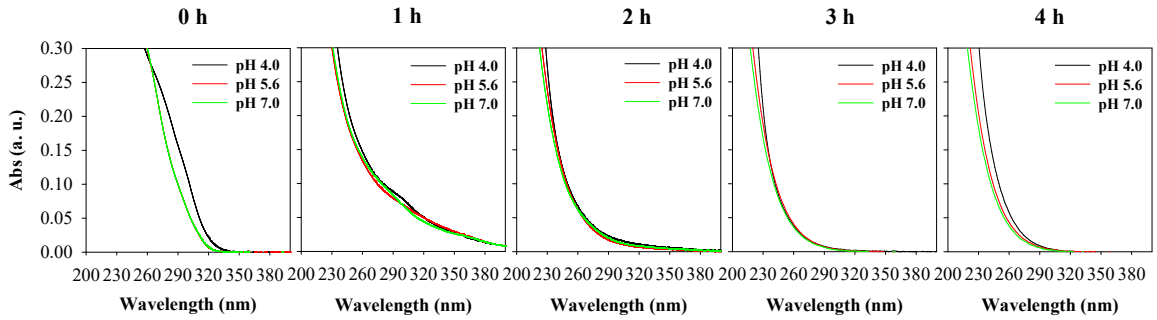

Figure 3.10: UV-Vis spectra (average spectra) during the oxidation of the mixture of contaminants by UV/H_2O_2, with $[H_2O_2]_0$ of 5 mM, at pH 4.0, 5.6 and 7.0, and for the reaction times reaction of: 0 h, 1 h, 2 h, 3 h and 4 h.

From the observation of the UV-Vis spectra, no relevant differences can be pointed out between the different pH's, which suggests that the oxidation of the mixture of contaminants might not be influenced by the pH of the solution.

Figure 3.11 shows the synchronous fluorescence spectra during the oxidation of the mixture by the UV/H_2O_2 process, at pH 4.0, 5.6 and 7.0, for the following reaction times: 0 h, 1 h, 2 h, 3 h and 4 h.

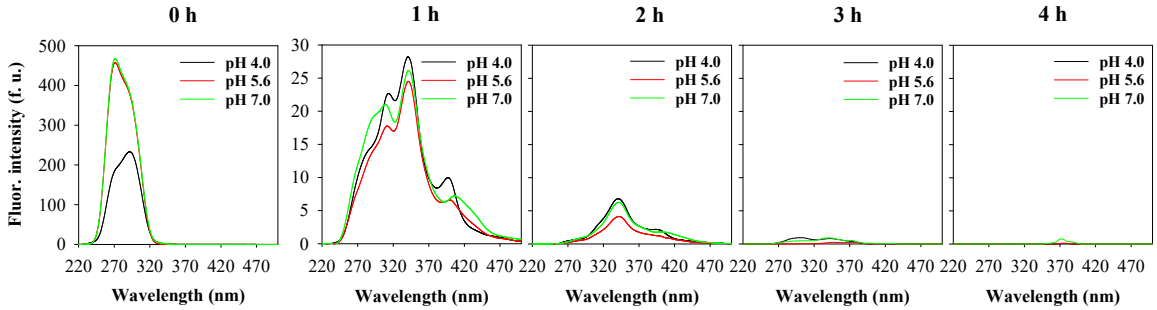

Figure 3.11: Synchronous fluorescence spectra (Δλ = 60 nm; average spectra) during the oxidation of the mixture of contaminants by UV/H_2O_2, with $[H_2O_2]_0$ of 5 mM, at pH 4.0, 5.6 and 7.0, and for the reaction times of: 0 h, 1 h, 2 h, 3 h and 4 h.

Figure 3.12 presents the EEM fluorescence spectra of the oxidation of the mixture by the UV/H_2O_2 process, at 0 h, 1 h, 2 h, 3 h and 4 h, and at the pH values of 4.0, 5.6 and 7.0.

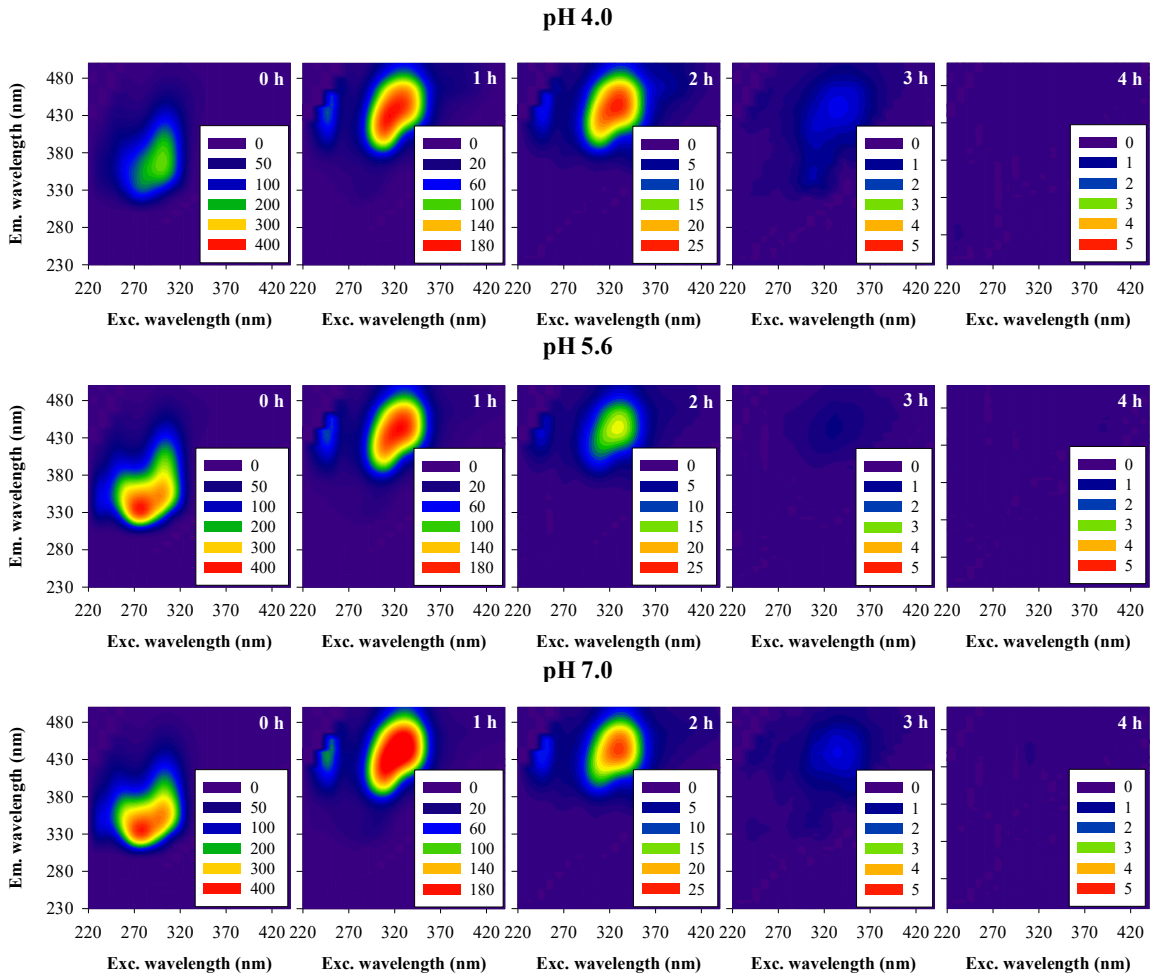

Figure 3.12: Excitation-emission matrix (EEM) fluorescence spectra (average spectra) during the oxidation of the mixture of contaminants by UV/H_2O_2, with $[H_2O_2]_0$ of 5 mM, at pH 4.0 (upper row), pH 5.6 (middle row) and pH 7.0 (bottom row), and for 0 h, 1 h, 2 h, 3 h and 4 h.

As shown in Figures 3.11 and 3.12, the synchronous and EEM fluorescence spectra of 0 h, at pH 4.0, display a lower intensity, when compared to pH 5.6 and 7.0, which means that the fluorescence of the mixture is pH dependent, which is a consequence of the protonation of the compounds. In this case, pH 4.0 has a higher degree of protonation, and presents a lower fluorescence intensity than the other pH's (Sharma & Schulman, 1999). However, with the course of the oxidation reaction, the spectra for the different pH's are very similar, which might mean that pH does not have an influence on the oxidation of the mixture. During the oxidation, the same compounds are formed, which is highlighted by the presence of the same fluorescence bands. It is noteworthy that those bands are present for the same reaction times in the spectra of each pH, and that, after 4 h, all chromophoric compounds were degraded, regardless of the pH.

In order to evaluate the differences between the pH's for each of the reaction times, the volume under the surface of the EEM fluorescence spectra was calculated for each reaction time, for pH 4.0, 5.6 and 7.0, and converted to extent of oxidation, according to Equation 2.1. The extents of oxidation for each reaction time (0 h, 1 h, 2 h, 3 h and 4 h), and for each pH value (4.0, 5.6 and 7.0) are presented in Figure 3.13.

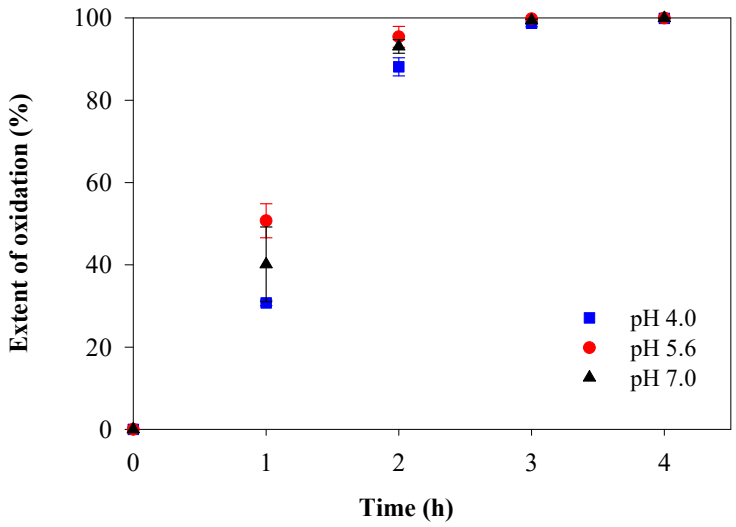

Figure 3.13: Extent of oxidation (%; average values) of the mixture of compounds during oxidation by UV/H_2O_2, with $[H_2O_2]_0$ of 5 mM, at pH 4.0, 5.6 and 7.0, and for the following reaction times: 0 h, 1 h, 2 h, 3 h and 4 h.

Figure 3.13 shows that the extents of oxidation are similar for the three pH's, except for pH 4.0 and pH 5.6 at the reaction times of 1 h and 2 h. After 1 h, the average extent of oxidation was 50.7 % at pH 5.6, and 30.8 % at pH 4.0. Afterwards, at 2 h, the average extent of oxidation was 95.4 % at pH 5.6, and 88.1 % at pH 4.0. Moreover, the extent of oxidation reached the maximum oxidation rate (at about 100 %) for the three pH's within 3 h of reaction.

The extents of oxidation obtained for each pH and time of reaction were compared using a two-sided Student's *t-test* for a significance level of 5 % ($\alpha = 0.05$). Before the application of the *t-test*, a *F-test* was performed to compare the variances of the results obtained for each pH and time of reaction, to determine if a *t-test* for equal or non-equal variances should be performed. Table 3.1 presents the results from the application of the *t-test* to the experimental data, namely information about the degrees of freedom (*df*), the calculated t value (t_{stat}), the critical t value (t_{crit}) and *p-values*.

Table 3.1: Results from the application of the t-test, for each reaction time (t; 1 h, 2 h, 3 h and 4 h), for pH 4.0, pH 5.6 and pH 7.0. The number of degrees of freedom (df), the calculated *t* value (t_{stat}), the critical *t* value (t_{crit}) and the p-value are also present.

t (h)	Compared group	*df*	t_{stat}	t_{crit}	*p-value*
1	pH 4.0 vs pH 5.6	3	5.23	3.18	0.014
	pH 4.0 vs pH 7.0	3	1.13	3.18	0.342
	pH 5.6 vs pH 7.0	4	1.50	2.78	0.208
2	pH 4.0 vs pH 5.6	4	3.06	2.78	0.038
	pH 4.0 vs pH 7.0	4	2.54	2.78	0.064
	pH 5.6 vs pH 7.0	4	1.08	2.78	0.339
3	pH 4.0 vs pH 5.6*	2	1.78	4.30	0.216
	pH 4.0 vs pH 7.0	4	1.02	2.78	0.367
	pH 5.6 vs pH 7.0*	2	1.67	4.30	0.237
4	pH 4.0 vs pH 5.6	4	1.44	2.78	0.222
	pH 4.0 vs pH 7.0*	2	0.98	4.30	0.432
	pH 5.6 vs pH 7.0	4	1.74	2.78	0.157

**t-test* for non-equal variances

Through the analysis of Table 3.1, it can be concluded that the null hypothesis, which states that there is no difference between the two means, can only be rejected for pH 4.0 vs pH 5.6, for the reaction times of 1 h and 2 h, since $t_{stat} > t_{crit}$ and $p\text{-}value < 0.05$. As discussed before, at a reaction time of 0 h, the EEM fluorescence spectrum presents a lower intensity when compared to the other two pH's. Since the extent of oxidation is calculated based on the integrated EEM fluorescence spectra volume, and uses the volume of the spectra of 0 h, the difference between pH 4.0 and 5.6, at the reaction times of 1 h and 2 h can be attributed to the difference in the spectra of 0 h. Nevertheless, when considering a significance level of 0.01, the null hypothesis cannot be rejected for pH 4.0 vs pH 5.6 for the reaction time of 1 h. Additionally, for pH 4.0 vs pH 5.6, at 2 h, the null hypothesis cannot be rejected at a significance level of 0.03. This way, there is no statistical evidence that the pH influences the oxidation of the mixture of compounds.

3.4 Optimization of the UV/H_2O_2 process on the oxidation of the mixture of contaminants

In order to optimize the UV/H_2O_2 process on the oxidation of the mixture of contaminants, an Uniform Design was selected, since within a small number of experiences, it is possible to explore the relationships between the factors and the response. The factors considered for the optimization of the oxidation of the mixture by UV/H_2O_2 were the reaction time, pH and initial H_2O_2 concentration. Therefore, three factors with three levels were used: 0.5 mM, 2.5 mM and 5.0 mM, for H_2O_2 concentration; 2 h, 4 h and 7 h, for reaction time; and 4.0, 5.6 and 7.0, for pH. The extent of oxidation, calculated as previously mentioned, was used as the response. Three replications of the experimental design were made, and the results, expressed as extent of oxidation, can be consulted in Table 3.2.

Table 3.2: Results from the experimental design, expressed as extent of oxidation (%) for the three replicates, and respective level for each factor ([H_2O_2], t, pH).

	Factors			**Extent of oxidation (%)**		
Run order	**$[H_2O_2]_0$ (mM)**	**t (h)**	**pH**	**First replica**	**Second replica**	**Third replica**
1	0.5	4	7.0	65.6	72.3	69.1
2	2.5	7	4.0	99.9	100.0	100.0
3	5.0	7	5.6	100.0	100.0	100.0
4	5.0	2	5.6	99.1	95.8	97.9
5	2.5	2	7.0	74.3	81.2	75.6
6	5.0	4	4.0	99.9	100.0	100.0
7	0.5	2	5.6	21.8	19.1	18.0
8	2.5	2	4.0	79.9	82.7	79.2
9	2.5	7	7.0	100.0	100.0	100.0
10	5.0	4	7.0	100.0	100.0	100.0
11	0.5	7	5.6	93.6	99.5	98.2
12	0.5	4	4.0	66.4	70.8	65.6

As it can be seen in the Table 3.2, the percentage of oxidation varied from 18.0 % to 100.0 %, and replicas did not present standard deviations higher than 3 %.

The Uniform Design, shown in Table 3.2, allowed the development of mathematical equations, where predicted results were assessed as a function of H_2O_2 concentration, time of reaction and pH. The better way to ensure that a chosen model is the one that better describes the data and is able to perform the best predictions, is to test all the possible models (Olejnik et al., 2000). However, this an arduous task, since there are too many possible combinations when multiple factors are considered (Olejnik et al., 2000), which is the case. For this reason, best subsets regression was employed. Best subsets regression compares all possible models that can be created based on a set of predictors, and presents the best models for one predictor, two predictors, three predictors, and so on, for the number of possible predictors. The regression analysis considered three first-order effects, initial H_2O_2 concentration ($[H_2O_2]_0$), time of reaction (t) and pH; three interaction effects, specifically, the interaction between H_2O_2 concentration and time of reaction ($[H_2O_2]_0 \times t$), between H_2O_2 concentration and pH ($[H_2O_2]_0 \times pH$), and between time of reaction and pH ($t \times pH$); and three second-order effects, $[H_2O_2]_0^2$, t^2 and pH^2, according to Equation 2.2. Table 3.3 illustrates the models suggested by best subsets regression, and the predictor variables considered in each model, as well as the associated *p-value*, and other statistical parameters, namely the *p-value*, coefficient of determination (R^2), adjusted R^2 (R^2_{adj}) and Mallow's C_p for each model.

Table 3.3: Models obtained by application of best subsets regression. Predictor variables and associated *p-value*, *p-value* of the model, R^2, R^2_{adj} and Mallow's C_p are presented for each model.

Model	Predictors	*p-value*	R^2	R^2_{adj}	C_p	*p-value* of predictors in the model								
						$[H_2O_2]$	t	pH	$[H_2O_2]^2$	t^2	pH^2	$[H_2O_2]\times t$	$[H_2O_2]\times pH$	$t\times pH$
1	$[H_2O_2]_0\times$ t	<0.001	0.400	0.382	202.3	-	-	-	-	-	-	<0.001	-	-
2	$[H_2O_2]_0$, t	<0.001	0.685	0.666	93.1	<0.001	<0.001	-	-	-	-	-	-	-
3	$[H_2O_2]_0$, t, $[H_2O_2]_0\times t$	<0.001	0.881	0.870	18.6	<0.001	<0.001	-	-	-	-	<0.001	-	-
4	$[H_2O_2]_0$, t, $[H_2O_2]_0^2$, $[H_2O_2]_0\times t$	<0.001	0.911	0.899	9.0	<0.001	<0.001	-	-	0.003	-	<0.001	-	-
5	$[H_2O_2]_0$, t, $[H_2O_2]_0^2$, t^2, $[H_2O_2]_0\times t$	<0.001	0.933	0.921	2.4	<0.001	<0.001	-	<0.001	0.004	-	<0.001	-	-
6	pH, t, $[H_2O_2]_0^2$, t^2, pH^2, $[H_2O_2]_0\times t$	<0.001	0.933	0.919	4.3	-	<0.001	<0.001	<0.001	<0.001	<0.001	<0.001	-	-
7	pH, t, $[H_2O_2]_0^2$, t^2, pH^2, $[H_2O_2]_0\times t$, $t\times pH$	<0.001	0.933	0.917	6.0	-	<0.001	<0.001	<0.001	<0.001	<0.001	<0.001	-	0.566
8	pH, t, $[H_2O_2]_0^2$, t^2, pH^2, $[H_2O_2]_0\times t$, $[H_2O_2]_0\times pH$, $t\times pH$	<0.001	0.933	0.914	8.0	-	0.003	<0.001	<0.001	<0.001	<0.001	<0.001	0.997	0.573

To determine the best model, the fit statistics presented in Table 3.3 were used in combination with one another. All models contemplated in the table are significant at a 95 % confidence level, since *p-values* are less than 0.05. However, when looking at the *p-value* of each predictor variable, for each model, it is possible to notice that models 7 and 8 display predictor variables with *p-values* higher than 0.05. This means that those predictor variables, namely t×pH for model 7, and $[H_2O_2]_0$×pH and t×pH for model 8, are not significant in the model in which they are predictors.

Values of R^2 close to 1 and higher than 0.8 are recommended for a good fit of a model (Manan et al., 2019), and imply that most of the variability in the dependent variable is explained by the regression model (Montgomery et al., 2001). The R^2 parameter increases by adding terms to the model, regardless of the contribution of that variable (Montgomery et al., 2001), which makes this parameter not suitable for the choice of the best model. Moreover, R^2 stabilized with more than 5 predictor variables. On the other hand, R^2_{adj} only increases by adding a variable to the model if the addition of the variable reduces the residual mean square (Montgomery et al., 2001), so it is more reasonable to use R^2_{adj}, as it only increases if the added predictors improve the model (Manan et al., 2019). When selecting the best subset, one must, then, look for the highest R^2_{adj}, which, in this case, is 0.921, for model 5. Nevertheless, models 6, 7 and 8 present similar R^2_{adj} values to the one of model 5, and models 3 and 4 present R^2_{adj} values higher than 0.8. Models 1 and 2, however, have poor R^2 values of 0.400 and 0.685, respectively.

Mallow's C_p should also be considered when choosing a model, for it is a measure of bias or prediction error. A study from Olejnik et al. (2000) even demonstrated that C_p has more success in identifying the authentic variables than R^2_{adj}. Generally, small values of C_p are desirable (Montgomery et al., 2001). In this case, the smallest value of Mallow's C_p belongs to model 5, which means that this model is more precise than the others.

Given that the smallest C_p and the highest R^2_{adj} values belong to model 5, this model was chosen as the "best", from the models resultant from the application of best subsets regression. As it can be seen in Table 3.3, only H_2O_2 concentration, reaction time, the interaction between these two and their quadratic forms are present in the model. This means that the initial pH of the solution is not significant for the oxidation of the mixture. This is in agreement with the previous section, where it was stated that there was no

statistical evidence to conclude that the pH had influence on the oxidation of the mixture of contaminants.

In Table 3.4, a summary of the chosen model is displayed, where information about the sum of squares, mean square, degrees of freedom, *F* and *p-values*, R^2 and R^2_{adj} are presented.

Table 3.4: Model summary, where *SS* stands for sum of squares, *DF* for degree of freedom, and *MS* for mean square. *F* and *p-values*, R^2, R^2_{adj} and the coefficients of each variable in the model are also present.

	SS	***DF***	***MS***	**Coefficient**	***F***	***p-value***	R^2	R^2_{adj}
Corrected model	17801	5	3560		82.9	<0.001	0.933	0.921
Intercept	425	1	425		9.90	0.004		
Constant				-31.20				
$[H_2O_2]$	4717	11	4717	35.01	110	<0.001		
t	1747	1	1747	26.82	40.7	<0.001		
$[H_2O_2]^2$	954	1	954	-2.526	22.2	<0.001		
t^2	420	1	420	-1.402	9.79	0.004		
$[H_2O_2]\times t$	3706	1	3706	-3.084	86.3	<0.001		
Error	1288	30	42.9					
Total	273301	36						
Corrected Total	19089	35						

As shown in Table 3.3 and in Table 3.4, the model presents a good fit to the experimental data, since the R^2_{adj} is 0.921, which means that 92.1 % of the results can be explained by the model. Moreover, the model has a high significance, since F_{crit} (2.53) < $F_{(5,30)}$ (82.9), and its *p-value* is inferior to 0.05 (*p-value* < 0.001). The sum of squares (*SS*) of the model and of each variable allowed the evaluation of their significance (*p-value* <

0.05). The residual sum of squares (error) is another important parameter, as the smaller the residual sum of squares is, the better the model fits the data.

The relationship between the extent of oxidation of the mixture and the independent variables is given by the following equation:

$$Extent\ of\ oxidation\ (\%) = -31.20 + 35.01 \times [H_2O_2] + 26.82 \times t - 2.526 \times [H_2O_2]^2 - 1.402 \times t^2 - 3.084 \times [H_2O_2] \times t \quad (3.1)$$

where $[H_2O_2]$ is the initial concentration of H_2O_2 (mM) and t is the reaction time (h). The coefficients in this equation reveal that the concentration of H_2O_2 and that the time of reaction have a positive influence on the extent of oxidation: an increase in the H_2O_2 concentration, or in the reaction time leads to higher percentages of extent of oxidation.

The extents of oxidation (%) were predicted using Equation 3.1, and the results were plotted against the real experimental values, as shown in Figure 3.14.

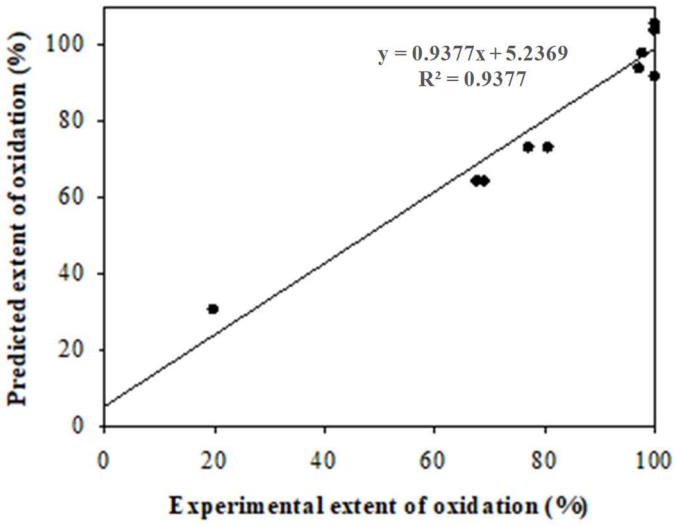

Figure 3.14: Comparison between predicted and experimental extents of oxidation (%).

The relationship between the predicted and experimental values of the extent of oxidation is linear ($R^2 = 0.9377$), and there is a strong correlation between the model's predictions and its actual results, which implies that the proposed model is adequate.

Figure 3.15 shows the response surface model obtained, and the experimental data, both plotted with the Working-Hotelling surface confidence intervals, at a 95 % confidence level.

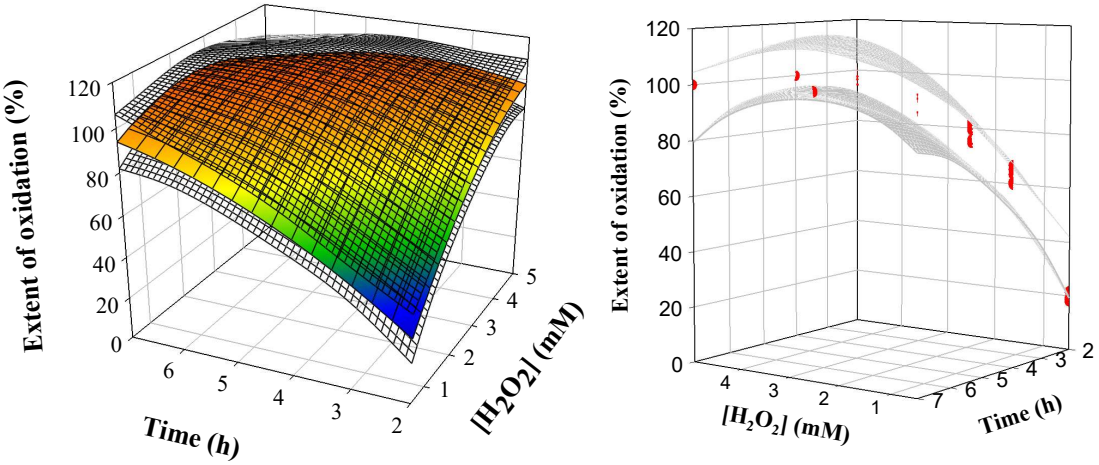

Figure 3.15: Response surface model with the associated Working-Hotelling surface confidence intervals at a 95 % confidence level (left); and experimental data with the Working-Hotelling surface confidence intervals at a 95 % confidence level (right).

As seen in Figure 3.15, at a reaction time of 2 h and at an H_2O_2 concentration of 0.5 mM, the response surface model presents a low percentage of extent of oxidation. As the H_2O_2 concentration increases, or as the reaction time increases, the extent of oxidation also increases. It is worth to mention that the mean values of the experimental data are within the surface confidence intervals. On the other hand, the individual values are within the confidence intervals, except for a concentration of H_2O_2 of 0.5 mM, a pH of 5.6 and a reaction time of 2 h, and for H_2O_2 of 2.5 mM, a pH of 4.0 and a reaction time of 2 h. However, the values that are out of the confidence intervals are not statistically different from the values that are contained within the intervals (Dixon's test; $\alpha = 0.05$).

Based on the equation obtained for the model (Equation 3.1), it is possible to optimize the extent of oxidation. In this case, an equilibrium between H_2O_2 concentration and reaction time was desired. The minimum H_2O_2 concentration for the maximum reaction time of 4 h, which translated into extents of oxidation equal or higher than 99.5%, was searched. This search resulted in an H_2O_2 concentration of 3.1 mM and a reaction time of 4 h.

3.5 Oxidation of the mixture of contaminants by the UV/H_2O_2 process in rainwater samples

In order to understand the effect of the oxidation of the mixture of contaminants by the UV/H_2O_2 process in rainwater samples, experiments with two rainwater samples spiked with the mixture of contaminants were performed at their natural pH, namely pH 5.2 and pH 5.4, for samples 1 and 2, respectively. These experiments were performed with a concentration of H_2O_2 of 5.0 mM, to allow the comparison with the previous results with the model solutions, for the following reaction times: 0 h, 2 h and 4 h. A reaction time of 4 h was chosen so that everything would surely be oxidized by the end of this time, similar to what was observed for model solutions. As control, the following experiments were performed: samples spiked with the mixture of contaminants, and without H_2O_2; samples with H_2O_2 at a concentration of 5.0 mM; and samples without H_2O_2. The UV-Vis spectra resultant from these experiments are presented in Figure 3.16.

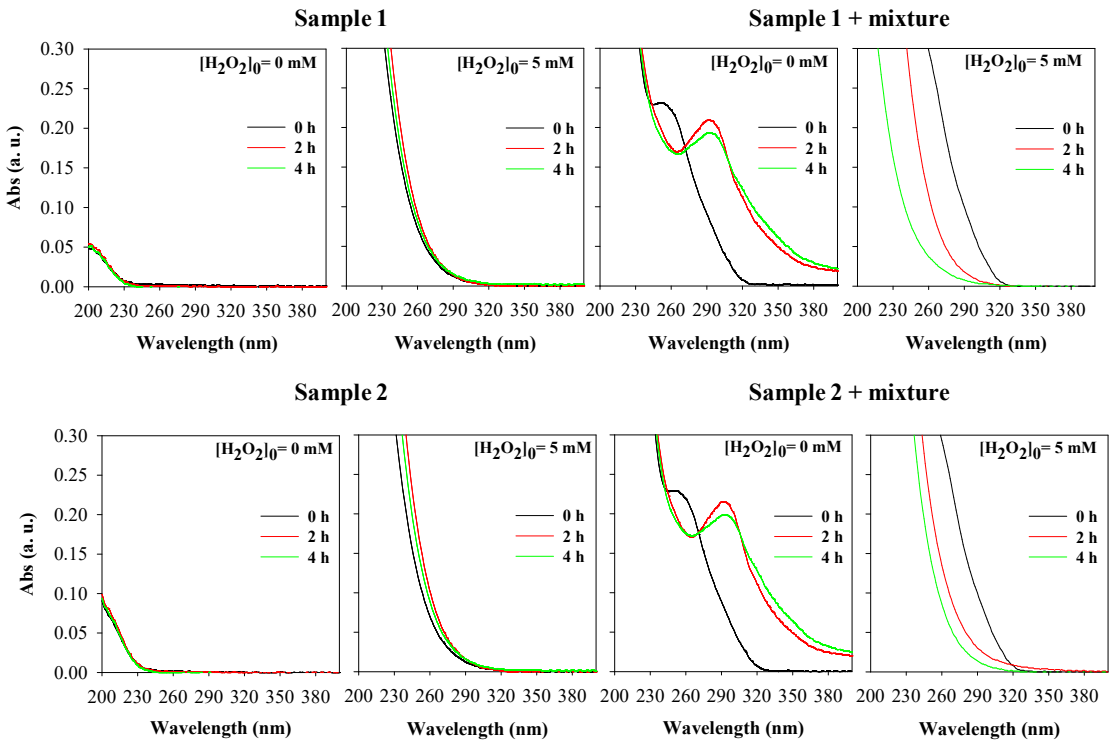

Figure 3.16: UV-Vis during the oxidation of rainwater samples 1 and 2 at their natural pH (5.2 and 5.4, for samples 1 and 2, respectively) and for 0 h, 2 h and 4 h: not spiked with the mixture of contaminants and H_2O_2 ($[H_2O_2]_0 = 0$ mM; by UV); not spiked with the mixture of contaminants, but spiked with H_2O_2 ($[H_2O_2]_0 = 5$ mM; by UV/H_2O_2); spiked with the mixture of contaminants, and not spiked with H_2O_2 ($[H_2O_2]_0 = 0$ mM; by UV); and spiked with the mixture of contaminants and H_2O_2 ($[H_2O_2]_0 = 5$ mM; by UV/H_2O_2).

Figure 3.16 shows that the UV-Vis spectra of the two samples (at 0 h for a concentration of H_2O_2 of 0 mM) are similar to those obtained by Santos et al. (2019) for rainwater samples, decreasing the absorbance of both samples as the wavelength increases. There are no changes with the time in the spectra that correspond to the experiments with samples not spiked with the mixture of contaminants and without H_2O_2, which reveals that there was no oxidation in this case. In the spectra obtained in the experiments with the addition of H_2O_2 to the samples, but without these being spiked with the mixture, the absorbance significantly increased when compared to the spectra without H_2O_2 (which was due to the presence of H_2O_2), but they did not change with the course of the reaction. Concerning the spectra resultant from the addition of the mixture of contaminants to the samples, but without H_2O_2, they reveal an absorption band at 252 nm at 0 h, which moves to a longer wavelength, 290 nm, after 2 h of reaction. After 4 h of reaction, its absorbance slightly diminishes. These alterations suggest that the compounds are being transformed, similar to what happened in the oxidation with model solutions, where the main absorbance band moved to longer wavelengths. Regarding the spectra obtained for the samples spiked with the mixture of contaminants when H_2O_2 was added in a concentration of 5 mM, it can be seen that, with the course of the reaction, the compounds are being degraded, as the absorbance of the spectra decreases with time. At a reaction time of 4 h, sample 1 seems to have been more oxidized than sample 2.

Similar to what was previous described, synchronous fluorescence spectra were also recorded for the experiments of oxidation of the samples. In Figure 3.17 are presented the spectra, obtained up to 4 h, for the experiments with samples not spiked with the mixture of contaminants and without H_2O_2, with samples not spiked with the mixture of contaminants and with H_2O_2 at a concentration of 5.0 mM, with samples spiked with the mixture but without H_2O_2, and with samples spiked with the mixture and with H_2O_2 at the concentration of 5.0 mM.

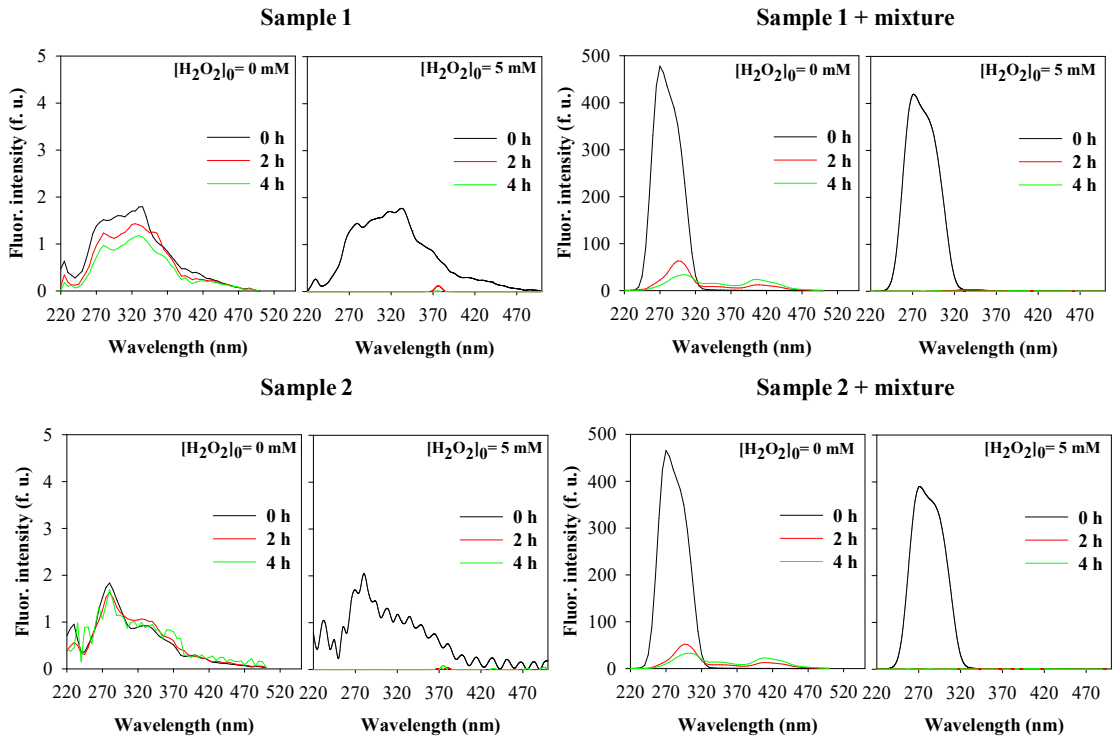

Figure 3.17: Synchronous fluorescence spectra ($\Delta\lambda$ = 60 nm) during the oxidation of rainwater samples 1 and 2 at their natural pH (5.2 and 5.4, for samples 1 and 2, respectively) and for 0 h, 2 h and 4 h: not spiked with the mixture of contaminants and H_2O_2 ($[H_2O_2]_0$ = 0 mM; by UV); not spiked with the mixture of contaminants, but spiked with H_2O_2 ($[H_2O_2]_0$ = 5 mM; by UV/H_2O_2); spiked with the mixture of contaminants, and not spiked with H_2O_2 ($[H_2O_2]_0$ = 0 mM; by UV); and spiked with the mixture of contaminants and H_2O_2 ($[H_2O_2]_0$ = 5 mM; by UV/H_2O_2).

Figures 3.18 and 3.19 display the EEM fluorescence spectra obtained during the oxidation of samples 1 and 2, and of samples 1 and 2 spiked with the mixture of contaminants, by UV/H_2O_2, and up to 4 h of reaction, as well as for the controls without H_2O_2.

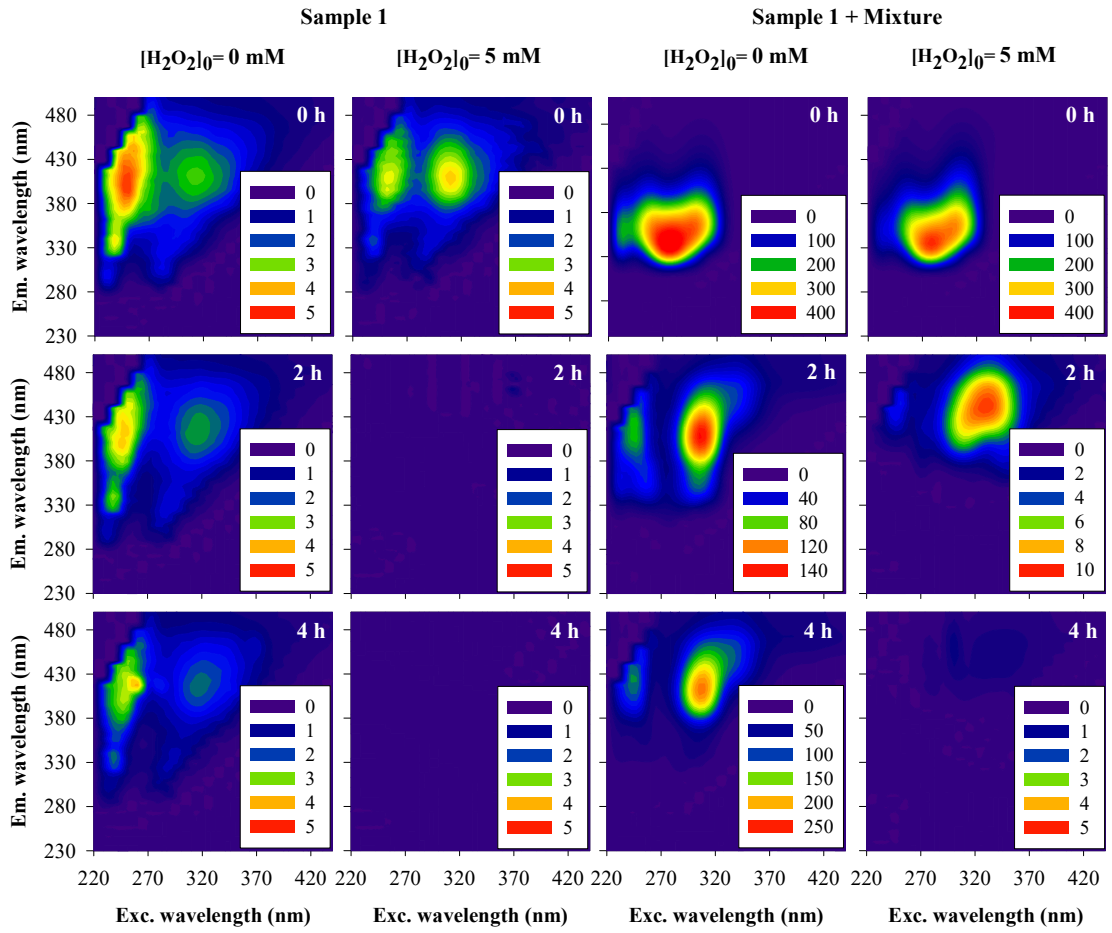

Figure 3.18: Excitation-Emission matrix (EEM) fluorescence spectra during the oxidation of rainwater samples 1 at its natural pH (5.2) and for 0 h, 2 h and 4 h: not spiked with the mixture of contaminants and H_2O_2 ($[H_2O_2]_0 = 0$ mM; by UV); not spiked with the mixture of contaminants, but spiked with H_2O_2 ($[H_2O_2]_0 = 5$ mM; by UV/H_2O_2); spiked with the mixture of contaminants, and not spiked with H_2O_2 ($[H_2O_2]_0 = 0$ mM; by UV); and spiked with the mixture of contaminants and H_2O_2 ($[H_2O_2]_0 = 5$ mM; by UV/H_2O_2).

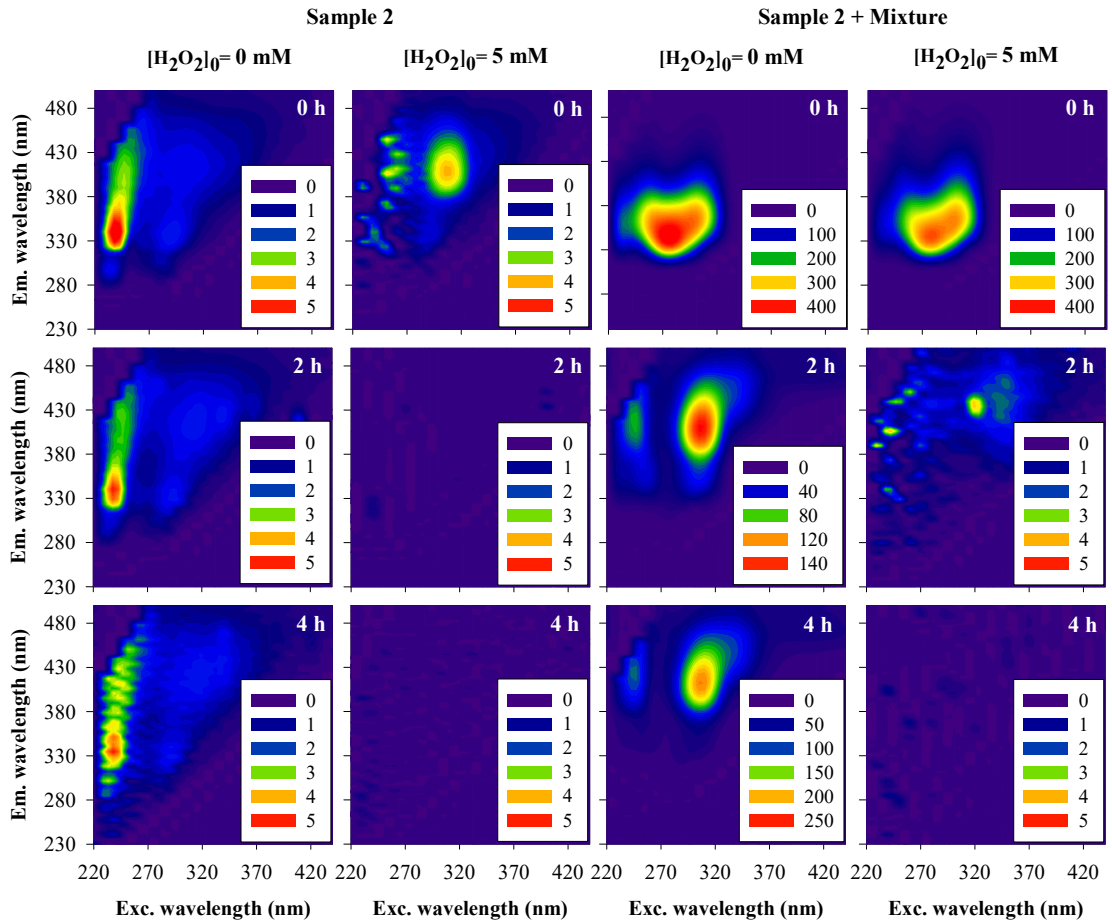

Figure 3.19: Excitation-Emission matrix (EEM) fluorescence spectra during the oxidation of rainwater sample 2 at its natural pH (5.4) and for 0 h, 2 h and 4 h: not spiked with the mixture of contaminants and H_2O_2 ($[H_2O_2]_0 = 0$ mM; by UV); not spiked with the mixture of contaminants, but spiked with H_2O_2 ($[H_2O_2]_0 = 5$ mM; by UV/H_2O_2); spiked with the mixture of contaminants, and not spiked with H_2O_2 ($[H_2O_2]_0 = 0$ mM; by UV); and spiked with the mixture of contaminants and H_2O_2 ($[H_2O_2]_0 = 5$ mM; by UV/H_2O_2).

The synchronous fluorescence spectra of both samples, not spiked with the mixture of contaminants, and without H_2O_2, showcase low intensities, which means that the samples do not present a high content of chromophoric compounds. Nevertheless, both samples appear to have a fluorescent band located at 270 nm and another one at 330 nm of excitation wavelength. In the case of sample 2, this last band appears as a shoulder. The EEM spectrum of samples 1 and 2 shows four fluorescent bands with a low fluorescent intensity, located as similar locations. One is located near 230 nm of excitation and 410 nm of emission wavelength, generally attributed to humic-like compounds (A); other is located near 290 nm of excitation and 420 nm of emission wavelength, generally assigned to marine humic-like compounds (M); and two bands located near 230 nm of excitation and 335 nm of emission wavelength and near 280 nm of excitation and 335 nm of emission wavelength, usually assigned to protein-like compounds, such as tryptophan

(T_1 and T_2, respectively) (Santos et al., 2013). The more intense band in Sample 1 is band A, and T_1 in Sample 2. Nevertheless, band A is more intense than band M in both samples.

Both the synchronous fluorescence spectra and the EEM spectra, resultant from the oxidation of the samples not spiked with the mixture and without H_2O_2, suggest that there was some oxidation of the compounds in solution, since their intensity decreased throughout time. When adding H_2O_2, after 2 h of reaction time, all chromophoric compounds were degraded, for both samples. In the case where the samples were spiked with a mixture of contaminants, but without H_2O_2 in solution, the fluorescence spectra of 0 h, suggest the presence of two fluorescent bands, one located at 270 nm of excitation and 335 nm of emission wavelength (that is also present in the synchronous spectra), and the other submerged in this one, which were also identified in the experiments with the model solutions. After 2 h, two new fluorescent bands appear, one located at 240 nm of excitation and 420 nm of emission, and other at 300 nm of excitation and 415 nm of emission wavelength, which also appear in the spectra of the oxidation of the model solutions, suggesting that the same compounds are being formed. After 4 h, the intensity of these bands increases, like in the case of the model solutions, meaning that there are more chromophoric compounds that fluoresce in that region being formed. These observations suggest that UV light, on its own, is able to oxidize the samples spiked with the mixture, at some extent. At last, the oxidation of the samples spiked with the mixture, by the UV/H_2O_2 process, conducted to the complete oxidation of the samples in 4 h, similar to what was observed for the model solutions. However, after 2 h of reaction, sample 2 seems to have been more degraded than sample 1, suggesting that the matrix could be influencing the oxidation. When comparing the spectra from the oxidation of the sample spiked with the mixture only by UV light, to those of the oxidation of the sample spiked with the mixture by the UV/H_2O_2 process, it is clear that UV light causes some oxidation, but that the addition of H_2O_2 significantly increases the rate of oxidation, due to the formation of hydroxyl radicals, that attack and degrade the compounds in solution.

The optimal conditions (3.1 mM for H_2O_2 concentration and 4 h for reaction time), found in the previous section in the optimization of the UV/H_2O_2 process for the oxidation of a mixture of contaminants, were also applied to the samples spiked with the mixture of contaminants. The experiments were performed in duplicates, at their natural pH values. The results expressed in percentages of extent of oxidation are present in Table 3.5.

Table 3.5: Extent of oxidation (%) for rainwater samples 1 and 2, spiked with the mixture of contaminants, obtained by the UV/H_2O_2 process with $[H_2O_2]_0$=3.1 mM and after 4 h, at their natural rainwater pH (5.2 and 5.4, for sample 1 and 2, respectively).

	Extent of oxidation (%)	
	Sample 1	**Sample 2**
First replica	99.7	99.5
Second replica	99.9	99.5

An average extent of oxidation of 99.8 % was obtained for sample 1, and of 99.5 % for sample 2. Moreover, the values obtained between replicas for each sample are in agreement. These results are in accordance to what was predicted by the equation of the model, obtained in the previous section, which estimates that with the optimum conditions an extent of oxidation higher than 99.5 % is obtained.

These findings suggest that the model obtained, for the aforementioned conditions (3.1 mM for H_2O_2 concentration and 4 h for reaction time), can be used for the oxidation of contaminants in real samples.

Chapter 4

Conclusions

A mixture of contaminants, small aromatic compounds (benzoic acid, 3,5-dihydroxybenzoic acid and syringic acid), was oxidised by the UV/H_2O_2 process in water model solutions and in rainwater, and the oxidation was evaluated by UV-Vis and fluorescence spectroscopies.

The UV-Vis and fluorescence spectra of the mixture of contaminants obtained during the oxidation by the UV/H_2O_2 process evidenced the formation of new chromophoric compounds, possibly with higher degree of unsaturation and hydroxylation. The spectra also evidenced that the formed compounds were then degraded. Moreover, the combined process of UV/H_2O_2 increased the rate of oxidation of the mixture of compounds when compared with the oxidation only by UV light, highlighting the importance of the oxidant H_2O_2, and consequently of the hydroxyl radicals that are formed and that attack the compounds, on the degradation of the contaminants.

The rate of oxidation of contaminants is affected by the initial H_2O_2 concentration, and, higher H_2O_2 concentrations, lead to higher oxidation rates. A total degradation of the chromophoric compounds present in the mixture of contaminants was achieved after 4 h, using an H_2O_2 concentration of 5 mM.

The effect of the initial pH of the solution was tested for acidic (4.0), neutral (5.6) and basic (7.0) pH values for atmospheric waters, and the oxidation of the mixture of compounds showed not be affected by the value of the initial pH of solution for a level of significance of 0.01.

The optimum conditions for the oxidation of the mixture of compounds by the UV/H_2O_2 process in water solutions were achieved via response surface model with confidence intervals. The uniform experimental design, with H_2O_2 concentration, pH and reaction time as factors, and with three levels for each factor, was used to acquire measurement data for the model. It was obtained a regression equation to predict and describe the experimental data using best subsets regression. Such equation is a second-order polynomial surface, where H_2O_2 concentration, reaction time, the interaction of these two factors, and their quadratic forms were considered as variables. The absence of the pH in the equation demonstrates that this variable does not have significance to the model. The obtained experimental data were generally comprised within the confidence intervals of the model. From the model, the optimum conditions to obtain an extent of oxidation higher than 99.5 % were found as being the initial H_2O_2 concentration of 3.1 mM and a reaction time of 4 h.

The oxidation of the mixture of contaminants by the UV/H_2O_2 process in rainwater samples resulted in similar outcomes to those obtained with the model solutions, having occurred their total oxidation up to 4 h, for the initial H_2O_2 concentration of 5 mM, and for the optimum conditions obtained by the model (the initial H_2O_2 concentration of 3.1 mM and a reaction time of 4 h). Thus, in one hand it can be pointed out that the rainwater matrix affected the oxidation of the mixture of contaminants. On the other hand, it can be pointed that the model was able to predict the extents of oxidation of contaminants in rainwater efficiently.

In this study, the oxidation of the mixture of contaminants was evaluated in what concerns to the chromophoric content (by UV-Vis and fluorescence spectroscopies), but it would also be important in the future to evaluate the oxidation of the non chromophoric content by UV/H_2O_2, which would allow to confirm whether the total oxidation of organic compounds is achieved. Moreover, in future work it would be also important to test this oxidation process in a larger scale.

The results from this work propose, for the first time, the use of the UV/H_2O_2 process for the oxidation of organic contaminants in rainwater. Therefore, this process could be considered as an alternative for rainwater treatment, in what concerns to the removal of organic contaminants, for its posterior use in buildings, for domestic purposes.

References

Albinet, A., Minero, C., & Vione, D. (2010). Phototransformation processes of 2,4-dinitrophenol, relevant to atmospheric water droplets. *Chemosphere*, *80*(7), 753–758.

Arsene, C., Olariu, R. I., & Mihalopoulos, N. (2007). Chemical composition of rainwater in the northeastern Romania , Iasi region (2003 – 2006). *Atmospheric Environment*, *41*, 9452–9467.

Avery, B., Willey, J. D., & Wilson, C. A. (1991). Formic and Acetic Acids in Coastal North Carolina Rainwater. *American Chemical Society*, *25*(85).

Avery, G. B., Kieber, R. J., Witt, M., & Willey, J. D. (2006). Rainwater monocarboxylic and dicarboxylic acid concentrations in southeastern North Carolina, USA, as a function of air-mass back-trajectory. *Atmospheric Environment*, *40*(9), 1683–1693.

Balmer, M. E., & Sulzberger, B. (1999). Atrazine Degradation in Irradiated Iron/Oxalate Systems: Effects of pH and Oxalate. *Environmental Science & Technology*, *33*(3), 2418–2424.

Bauer, H., Claeys, M., Vermeylen, R., Schueller, E., Weinke, G., Berger, A., & Puxbaum, H. (2008). Arabitol and mannitol as tracers for the quantification of airborne fungal spores. *Atmospheric Environment*, *42*, 588–593.

Baxendale, J. H., & Magee, J. (1954). The photochemical oxidation of benzene in aqueous solution by ferric ion. *Transactions of the Faraday Society*, *51*, 205–213.

Bokare, A. D., & Choi, W. (2014). Review of iron-free Fenton-like systems for activating H2O2in advanced oxidation processes. *Journal of Hazardous Materials*, *275*, 121–135.

Boris, A. J., Desyaterik, Y., & Collett, J. L. (2015). Reprint of "How do components of real cloud water affect aqueous pyruvate oxidation?" *Atmospheric Research*, *151*, 52–63.

Carteau, D., & Pichat, P. (2010). Degradation of an ether-alcohol (3-ethoxyproan-1-ol) by photo-Fenton-generated OH radicals: products analysis and formation pathways; relevance to atmospheric water-phase chemestry. *Research of Chemical Intermediates*, *36*, 141–153.

Czuczwa, J., Leuenberger, C., & Giger, W. (1988). Seasonal and temporal changes of organic compounds in rain and snow. *Atmospheric Environment*, *22*(5), 907–916.

Deming, S. N., & Morgan, S. L. (1987). *Experimental design: a chemometric approach* (1st ed.). Amsterdam: Elsevier.

Deng, Y., Zhang, K., Chen, H., Wu, T., Krzyaniak, M., Wellons, A., Bolla, D., Douglas, K., Zuo, Y. (2006). Iron-catalyzed photochemical transformation of benzoic acid in atmospheric liquids: Product identification and reaction mechanisms. *Atmospheric Environment*, *40*, 3665–3676.

Downes, A., & Blunt, T. P. (1879). The effect of sunlight upon hydrogen peroxide. *Nature*, *28*, 521.

Fenton, H. J. H. (1894). Oxidation of tartaric acid in presence of iron. *Journal of the Chemical Society*, *65*, 899–910.

Flues, M., Hama, P., Lemes, M. J. L., Dantas, E. S. K., & Fornaro, A. (2002). Evaluation of the rainwater acidity of a rural region due to a coal-fired power plant in Brazil. *Atmospheric Environment*, *36*, 2397–2404.

Graham, B., Mayol-Bracero, O. L., Guyon, P., Roberts, G. C., Decesari, S., Facchini, M. C., Artaxo, P., Maenhaut, W., Koll, P., Andreae, M. O. (2002). Water-soluble organic compounds in biomass burning aerosols over Amazonia 1.Characterization by NMR and GC-MS. *Journal of Geophysical Research*, *107*(D20), 8047.

Guillard, C., Charton, N., & Pichat, P. (2003). Degradation mechanism of t-butyl methyl ether (MTBE) in atmospheric droplets. *Chemosphere*, *53*, 469–477.

Guo, L., Bao, L., She, J., & Zeng, E. Y. (2014). Significance of wet deposition to removal of atmospheric particulate matter and polycyclic aromatic hydrocarbons A case study in Guangzhou, China. *Atmospheric Environment*, *83*, 136–144.

Guo, L., & Lee, H. K. (2011). Low-density solvent-based solvent demulsification dispersive liquid-liquid microextraction for the fast determination of trace levels of sixteen priority polycyclic aromatic hydrocarbons in environmental water samples. *Journal of Chromatography A*, *1218*(31), 5040–5046.

Hardwick, T. J. (1957). The rate constant of the reaction between ferrous ions and hydrogen peroxide in acid solution. *Canadian Journal of Chemistry*, *35*, 428–436.

Kasiri, M. B., Aleboyeh, H., & Aleboyeh, A. (2008). Modeling and Optimization of Heterogeneous Photo-Fenton Process with Response Surface Methodology and Artificial Neural Networks. *Environ. Sci. Technol.*, *42*(21), 7970–7975.

Kawamura, K., & Kaplan, I. R. (1986). Biogenic and anthropogenic organic compounds in rain and snow samples collected in southern California. *Atmospheric Environment*, *20*(1), 115–124.

Lee, C., & Yoon, J. (2004). Temperature dependence of hydroxyl radical formation in the hv/Fe3+/H2O2 and Fe3+/H2O2 systems. *Chemosphere*, *56*(10), 923–934.

Liu, Y., Liu, L., Lin, J. M., Tang, N., & Hayakawa, K. (2006). Distribution and characterization of polycyclic aromatic hydrocarbon compounds in airborne particulates of East Asia. *China Particuology*, *4*(6), 283–292.

Lumbaque, E. C., Araújo, D. S., Klein, T. M., Tiburtius, E. R. L., Arguello, J., & Sirtori, C. (2019). Solar photo-Fenton-like process at neutral pH: Fe(III)-EDDS complex formation and optimization of experimental conditions for degradation of pharmaceuticals. *Catalysis Today*, *328*, 259-266.

Mack, J., & Bolton, J. R. (1999). Photochemistry of nitrite and nitrate in aqueous solution: a review. *Journal of Photochemistry and Photobiology A: Chemistry*, *128*, 26–38.

Manan, T. S. B. A., Khan, T., Sivapalan, S., Jusoh, H., Sapari, N., Sarwono, A., Ramli, R. M., Harimurti, S., Beddu, S., Sadon, S. N., Kamal, N. L. M., Malakahmad, A. (2019). Application of response surface methodology for the optimization of polycyclic aromatic hydrocarbons degradation from potable water using photo-Fenton oxidation process. *Science of the Total Environment*, *665*, 196–212.

Massart, D. L., Vandeginste, B. G. M., Buydens, L. M. C., Jong, S. De, Lewi, P. J., & Smeyers-Verbeke, J. (1997). *Handbook of Chemometrics and Qualimetrics Part A*. Amsterdam: Elsevier.

Milburn, R. M., & Vosburgh, W. C. (1955). A spectrophotometric Study of the

Hydrolysis of Iron (III) Ion. II. Polynuclear Species. *Journal of the American Chemical Society*, *77*(5), 1352–1355.

Mimura, A. M. S., Almeida, J. M., Vaz, F. A. S., Oliveira, M. A. L., Ferreira, C. C. M., & Silva, J. C. J. (2016). Chemical composition monitoring of tropical rainwater during an atypical dry year. *Atmospheric Research*, *169*, 391–399.

Montgomery, D. C., Peck, E. A., & Vining, G. G. (2001). *Introduction to linear regression analysis* (3rd ed.). New York: John Wiley & Sons, Inc.

Mullaugh, K. M., Byrd, J. N., Avery, G. B., Mead, R. N., Willey, J. D., & Kieber, R. J. (2014). Characterization of carbohydrates in rainwater from the Southeastern North Carolina. *Chemosphere*, *107*, 51–57.

Mullaugh, K. M., Hamilton, J. M., Avery, G. B., Felix, J. D., Mead, R. N., Willey, J. D., & Kieber, R. J. (2015). Chemosphere Temporal and spatial variability of trace volatile organic compounds in rainwater. *Chemosphere*, *134*, 203–209.

Okochi, H., Sugimoto, D., & Igawa, M. (2004). The enhanced dissolution of some chlorinated hydrocarbons and monocyclic aromatic hydrocarbons in rainwater collected in Yokohama, Japan. *Atmospheric Environment*, *38*(26), 4403–4414.

Olejnik, S., Mills, J., & Keselman, H. (2000). Using Wherry's Adjusted R and Mallow's Cp for Model Selection From All Possible Regressions. *The Journal of Experimental Education*, *68*(4), 365–380.

P. G. Hoel. (1971). *Introduction to Mathematical Statistics* (4th ed.). New York (NY): John Wiley & Sons, Inc.

Panin, G. N. (1990). Properties of Atmospheric Water. In *Encyclopedia of Life Support Systems* (Vol. I, pp. 1–10).

Pignatello, J. J., Oliveros, E., & MacKay, A. (2006). Advanced oxidation processes for organic contaminant destruction based on the fenton reaction and related chemistry. *Critical Reviews in Environmental Science and Technology*, *36*(1), 1–84.

Pruppacher, H. R., & Klett, J. D. (1978). *Microphysics of Clouds and Precipitation*. (1st ed.) London: Springer.

Rahman, M. M., Rahman, M. A., Haque, M. M., & Rahman, A. (2019). *Sustainable Water Use in Construction*. *Sustainable Construction Technologies*. Elsevier Inc.

Ruppert, G., Bauer, R., & Heisler, G. (1993). The photo-Fenton reaction - an effective photochemical wastewater treatment process. *Journal of Photochemistry and Photobiology A: Chemistry*, *73*, 75–78.

Safarzadeh-Amiri, A., Bolton, J. R., & Cater, S. R. (1996). The Use of Iron in Advanced Oxidation Processes. *Solarchem Environmental Systems*, *1*(1), 18–26.

Salar-Garcís, M. J., Ortiz-Martínez, V. M., Hernández-Fernández, F. J., Ríos, A. P. de los, & Quesada-Medina, J. (2016). Ionic liquid technology to recover volatile organic compounds (VOCs): A critical review. *Journal of Hazardous Materials*.

Santos, G. T. A. D., Santos, P. S. M., & Duarte, A. C. (2016b). Vanillic and syringic acids from biomass burning: Behaviour during Fenton-like oxidation in atmospheric aqueous phase and in the absence of light. *Journal of Hazardous Materials*, *313*, 201–208.

Santos, P. S. M., Cardoso, H. B., Rocha-Santos, T. A. P., & Duarte, A. C. (2019).

Oxidation of benzoic acid from biomass burning in atmospheric waters. *Environmental Pollution*, *244*, 693–704.

Santos, P. S. M., Domingues, M. R. M., & Duarte, A. C. (2016a). Fenton-like oxidation of small aromatic acids from biomass burning in atmospheric water and in the absence of light: Identification of intermediates and reaction pathways. *Chemosphere*, *154*, 599–603.

Santos, P. S. M., & Duarte, A. C. (2015). Fenton-like oxidation of small aromatic acids from biomass burning in water and in the absence of light: Implications for atmospheric chemistry. *Chemosphere*, *119*, 786–793.

Santos, P. S. M., Duarte, R. M. B. O., & Duarte, A. C. (2009). Absorption and fluorescence properties of rainwater during the cold season at a town in Western Portugal. *Journal of Atmospheric Chemistry*, *62*, 45–57.

Santos, P. S. M., Santos, E. B. H., & Duarte, A. C. (2014). Dissolved organic and inorganic matter in bulk deposition of a coastal urban area: An integrated approach. *Journal of Environmental Management*, *145*, 71–78.

Sarrai, A. E., Hanini, S., Merzouk, N. K., Tassalit, D., Szabó, T., Hernádi, K., & Nagy, L. (2016). Using Central Composite Experimental Design to Optimize the Degradation of Tylosin from Aqueous Solution by Photo-Fenton Reaction. *Materials*, *9*(428), 1–11.

Seinfeld, J. H., & Pandis, S. N. (2006). *Atmospheric Chemistry and Physics: From Air Pollution to Climate Change* (2nd ed.). New Jersey: John Wiley & Sons, Inc.

Sharma, A., & Schulman, S. G. (1999). *Introduction to fluorescence spectroscopy*. New York (NY): John Wiley & Sons, Inc.

Simoneit, B. R. T. (2002). Biomass burning - a review of organic tracers for smoke from incomplete combustion. *Applied Geochemistry*, *17*, 129–162.

Tang, A., Zhuang, G., Wang, Y., Yuan, H., & Sun, Y. (2005). The chemistry of precipitation and its relation to aerosol in Beijing. *Atmospheric Environment*, *39*, 3397–3406.

Tsai, Y. I., Kuo, S., Young, L., Hsieh, L., & Chen, P. (2014). Atmospheric dry plus wet deposition and wet-only deposition of dicarboxylic acids and inorganic compounds in a coastal suburban environment. *Atmospheric Environment*, *89*, 696–706.

Vione, D., Maurino, V., Minero, C., Duncianu, M., Olariu, R. I., Arsene, C., Sarakha, M., Mailhot, G. (2009). Assessing the transformation kinetics of 2- and 4-nitrophenol in the atmospheric aqueous phase. Implications for the distribution of both nitroisomers in the atmosphere. *Atmospheric Environment*, *43*(14), 2321–2327. https://doi.org/10.1016/j.atmosenv.2009.01.025

Vione, D., Maurino, V., Minero, C., Pelizzetti, E., Harrison, M. A. J., Olariu, R., & Arsene, C. (2006). Photochemical reactions in the tropospheric aqueous phase and on particulate matter. *Chemical Society Reviews*, *35*, 441–453.

Walling, C., & Weil, T. (1974). The Ferric Ion Catalyzed Decomposition of Hydrogen Peroxide in Perchloric Acid Solution. *Journal of Chemical Kinetics*, *6*, 507–516.

Williams, D. H., & Fleming, I. (1989). *Spectroscopic methods in organic chemistry* (4th ed.). London: McGraw-Hill.

Xing, L., & Chameides, W. L. (1990). Model Simulations of Rainout and Washout from

a Warm Stratiform Cloud. *Journal of Atmospheric Chemistry*, *10*, 1–26.

Zuo, Y., & Deng, Y. (1997). Iron(II)-Catalyzed Photochemical Decomposition of oxalic acid and generation of H2O2 in Atmospheric Liquid Phases. *Chemosphere*, *35*(9), 2051–2058.

Zuo, Y., & Hoigné, J. (1994). Photochemical decomposition of oxalic, glyoxalic and pyruvic acid catalysed by iron in atmospheric waters. *Atmospheric Environment*, *28*(7), 1231–1239.

Zuo, Y., & Holgné, J. (1992). Formation of Hydrogen Peroxide and Depletion of Oxalic Acid in Atmospheric Water by Photolysis of Iron(III)-Oxalato Complexes. *Environmental Science & Technology*, *26*(5), 1014–1022.

Zuo, Y., Zhang, K., Wu, J., Men, B., & He, M. (2011). Chemosphere Determination of o-phthalic acid in snow and its photochemical degradation by capillary gas chromatography coupled with flame ionization and mass spectrometric detection. *Chemosphere*, *83*(7), 1014–1019.

Appendix A – Statistical tests

A.1 *F*-test

Before the application of the *t* distribution, to test the difference between two means, it is necessary to test the equality of the two variances (Hoel, 1971). A statistical *F*-test that uses an *F* statistic can be used for this purpose.

The usual null hypothesis (H_0) is that the two population variances (σ_X and σ_Y) are equal (Hoel, 1971):

$$H_0: \sigma_X = \sigma_Y \qquad (A.1)$$

And the usual alternative hypothesis (H_1) is that the two population variances are unequal (Hoel, 1971):

$$H_1: \sigma_X \neq \sigma_Y \qquad (A.2)$$

Let X and Y be normally distributed and let S_X^2 and S_Y^2 be the variances of the two samples, of sizes n_X and n_Y, respectively (Hoel, 1971). Then,

$$F = \frac{S_X^2}{S_Y^2} \qquad (A.3)$$

will possess an *F* distribution, with $n_X - 1$ and $n_Y - 1$ degrees of freedom (Hoel, 1971). To test the null hypothesis, it is required to calculate the value of *F* and to consult tables of critical values of the *F*-distribution, to decide whether the value of *F* is unreasonably large or small on the desired significance level (Hoel, 1971), and therefore, we reject the null hypothesis if $F > F_{critical}$.

A.2 Student's *t*-test for comparison of two means

Student's *t*-tests are parametric tests based on the Student's or *t*-distribution (Hoel, 1971). For a comparison of means of two independent normal populations with unknown variances, a two-sample *t*-test, for equal or unequal variances, should be used.

The usual null hypothesis (H_0) is that the two population means (μ_X and μ_Y) are equal (Hoel, 1971):

$$H_0: \mu_X = \mu_Y \qquad (A.4)$$

And the usual alternative hypothesis (H_1) is that the two population means are unequal (Hoel, 1971):

$$H_1: \mu_X \neq \mu_Y \qquad (A.5)$$

A.2.1 *t*-test for equal variances

Let $\bar{X}$ and $\bar{Y}$ be the sample means of two sets of data of size n_X and n_Y, respectively, with the same variance (σ^2; Hoel, 1971). Let X and Y have a normal distribution or let n_X and n_Y be sufficiently large for the Central Limit Theorem to hold. Then, the random variable is given by

$$t = \frac{(\bar{X} - \bar{Y})}{S_p\sqrt{\frac{1}{n_X} + \frac{1}{n_Y}}} \qquad (A.6)$$

where S_p^2 is the pooled estimator of common variance σ^2, given by

$$S_p^2 = \frac{(n_X - 1) \times S_X^2 + (n_Y - 1) \times S_Y^2}{(n_X - 1) + (n_Y - 1)} \qquad (A.7)$$

where S_X^2 and S_Y^2 are the variances of X and Y, respectively (Hoel, 1971). t will have Student's *t* distribution with $n_X + n_Y - 2$ degrees of freedom (Hoel, 1971).

To test the null hypothesis, it is only necessary to calculate the value of *t* and use a Student's *t* distribution table to see whether the sample value of *t* numerically exceeds the critical value (Hoel, 1971). For instance, we reject the null hypothesis that both population means are equal ($H_0: \mu_X = \mu_Y$) if $|t| \geq t_{n_X+n_Y-2}(\frac{\alpha}{2})$.

A.2.2. *t*-test for unequal variances

Let $\bar{X}$ and $\bar{Y}$ be the sample means of two sets of data of size n_X and n_Y, respectively (Hoel, 1971). Let X and Y have a normal distribution or let n_X and n_Y be sufficiently large for the Central Limit Theorem to hold. Then, the random variable is given by

$$t = \frac{(\bar{X} - \bar{Y})}{\sqrt{\frac{S_X^2}{n_X} + \frac{S_Y^2}{n_Y}}} \qquad (A.8)$$

where S_X^2 and S_Y^2 are the variances of X and Y, respectively (Hoel, 1971). t will have Student's t distribution of $t(v)$, where the degrees of freedom are estimated as (Hoel, 1971):

$$v = \frac{\left(\frac{s_X^2}{n_X} + \frac{s_Y^2}{n_Y}\right)^2}{\frac{\left(\frac{s_X^2}{n_X}\right)^2}{(n_X - 1)} + \frac{\left(\frac{s_Y^2}{n_Y}\right)^2}{(n_Y - 1)}} \qquad (A.9)$$

The test procedure is to calculate the value t of the test statistics given by (A.8) and degrees of freedom, v, according to (A.9). Then, given the level of significance α, one should use the obtained v and Student's distribution to calculate critical value $t_v(\alpha)$ and draw conclusions comparing t and $t_v(\alpha)$ (Hoel, 1971).

A.3 Dixon's *Q* test

Dixon's Q test is a test to assess if suspected data belong to a population (Massart et al., 1997). Dixon's Q value is defined as the ratio of the difference between the suspected outlier and the closest to this value, and the difference between the largest and the smallest values of the set (Massart et al., 1997).

Considering a set of n data x_i $(i = 1, 2, \dots, n)$, arranged in ascending order, the Q value, depending if x_1 or x_n is the suspected value, is calculated according to (Massart et al., 1997):

$$Q = \frac{x_2 - x_1}{x_n - x_1} \; or \; Q = \frac{x_n - x_{n-1}}{x_n - x_1} \qquad (A.10)$$

The calculated Q value is, then, compared to the critical Q value, for a desired level of confidence (Massart et al., 1997). If the calculated Q value is not greater than the critical Q value, the questionable point is kept, otherwise, it is rejected (Massart et al., 1997).

Appendix B - Oxidation of the mixture of contaminants by UV

Figure B.1 shows the UV-Vis and synchronous fluorescence spectra obtained during the oxidation of the mixture of contaminants during the oxidation with UV light, at pH 5.6, for: 0 h, 2 h, 4 h and 7 h.

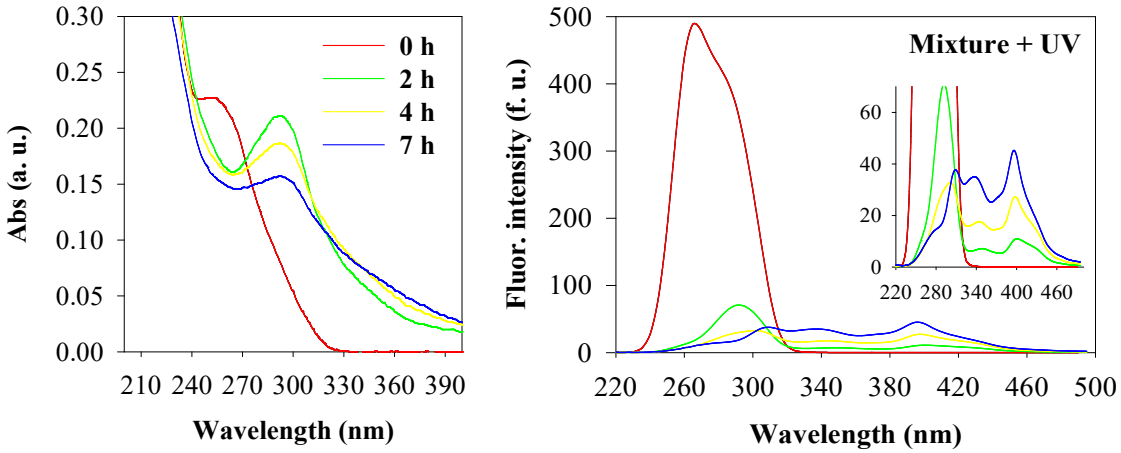

Figure B.1: UV-Vis and synchronous fluorescence spectra ($\Delta\lambda$ = 60 nm) of the mixture of the three contaminants during the oxidation with UV, at pH 5.6 and for the following oxidation times: 0 h, 2 h, 4 h and 7 h (left). The legend contained inside the UV-Vis spectra applies to both graphics.